Supplementary Methods

Flow-cytometric analysis

For analysis of mGFP expression by microscopy, HSCs were plated in chamber slides and maintained for 16h in DMEM media containing 10% FBS and antibiotics. For flow-cytometric analysis of mGFP expression, HSCs were analyzed on a FACSAria cell sorter based on vitamin A fluorescence to gate high purity HSCs, and mGFP expression to detect HSCs marked by Vim-CreER, providing a percentage of mGFP-positive cells among all Vitamin A-positive cells. For the analysis of mRNA expression, HSCs were sorted on a FACSAria cell sorter based on vitamin A fluorescence to gate high purity HSCs, and in some cases mGFP expression, and immediately lysed in RNA lysis buffer.

Bone marrow transplantation. Bone marrow transplantation was performed as previously described [1]. Briefly, mice underwent lethal irradiation with 2x6Gy followed by intravenous injection of $10x10^6$ bone marrow cells and reconstitution for at least 2 months following transplantation.

Microarray analysis. Microarray analysis of quiescent HSCs (n=4 independent HSC isolates) and reverted HSCs (n=4 independent isolates) was performed using Affymetrix 1.0ST chips according to the manufacturers instructions. Briefly, 150 ng total RNA was used for cDNA sythesis and terminal labeling using the Ambion WT expression and terminal labeling kit and Robust Multichip Algorithm normalization [2]. Data was deposited in GEO (Accession number: GSE38648). Differential expression was obtained using Limma [3] in the R/Bioconductor statistical computing environment [4]. A significance cutoff of the Benjamini-Hochberg False Discovery Rate <0.05 was used [5]. Complete linkage hierarchical clustering [6] was performed on significant genes with $|\log_2 FC| > 0.67$ using Cluster 3.0 [7] and JavaTreeview [8]. Pathway analysis was done by IPA Ingenuity using genes selecting by the above criteria, i.e. False Discovery Rate <0.05 and $|\log_2 FC|$ >0.67.

Immunohistochemistry and confocal microscopy

Immunohistochemical staining was done on frozen sections using primary antibodies against vimentin (1:100, Epitomics, Burlingame, CA, USA), desmin (1:200, Lab Vision, Thermo Fisher Scientific, Fremont, CA, USA), F4/80 (1:200, AbD Serotec, Raleigh, NC, USA), rabbit-anti cow pankeratin ("wide spectrum screening", 1:200, DAKO, Carpinteria, CA, USA), CD31 (1:200, Pharmingen, San Diego, CA) and HNF4α (1:100, Santa Cruz Biotechnology, Santa Cruz, CA, USA), and secondary Alexa Fluor 647 goat anti-rabbit, chicken anti-rat or Alexa Fluor 660 donkey anti-goat (Invitrogen, Carlsbad, CA, USA). Confocal microscopy was performed on a Nikon A1R MP confocal microscope (Nikon Instruments, Melville, NY, USA) using a 40x oil immersion lens. For some pictures, 4-6 40x sections were merged.

mGFP quantification

mGFP expression in purified HSCs was quantified 16h after plating. mGFP and Vitamin A fluorescence and phase contrast images were visualized an Olympus 71IX microscope using a 10x lens. Vitamin A-positive cells, mGFP-positive cells and VitaminA-mGFP double-positive cells were counted in Adobe Photoshop. mGFP expression was detected in frozen liver sections by confocal microscopy and analyzed by Image J. Data is expressed as percentage of mGFP area in comparison to total area.

Quantitative Real-time and Single Cell PCR

After column purification of RNA (RNeasy, Qiagen), DNAse treatment and reverse transcription, mRNA levels of Acta2, Col1a1, Col1a2, Desmin, Lox and Timp1 were determined by quantitative real-time PCR on an Applied Biosystem 7300 PCR cycler using ABI Taqman primers and probes as described.[9,10] For single cell PCR, single HSCs were flow-cytometrically sorted, using Vitamin A autofluorescence and excluding dead cells by propidium iodide staining, into 96-well plates containing a 9 µl mix of RT buffer from the Invitrogen CellsDirectTM One−Step qRT−PCR kit (Invitrogen, Carlsbad, CA, USA) and primers for pre-amplification. For the construction of standard curves, 1000 HSCs were sorted into some wells. Reverse transcription and 18 cycles of pre-amplification were immediately performed after cell sorting using the CellsDirectTM One−Step qRT−PCR kit. The ensuing qPCR was performed as described above using the 7300 Applied Biosystems PCR cycler and Taqman probes. Single cell qPCR was normalized to desmin, and only desmin-positive wells were used for qPCR analysis.

Statistical analysis

All data is expressed as means with error bars representing the standard deviation. Statistical calculations were performed using Prism (Graphpad, San Diego California, USA). For comparison of two groups, two-sided unpaired t-test or Mann-Whitney test were used. For multiple group comparisons with normal distribution, ANOVA with Neuman-Keuls or Dunnett posthoc analysis was performed. A p-value < 0.05 was considered statistically significant.

Supplementary Figure legends.

Supplementary Figure 1. HSCs were isolated from male untreated Balb/c mice or from Balb/c mice treated with 4 injections of CCl_4 and sacrificed at various time points after the last CCl_4 injection for the analysis of fibrogenic genes Col1a1, Col1a2, αSMA and TIMP1.

Supplementary Figure 2. A. Balb/c mice were treated with 12 intraperitoneal injections of TAA or left untreated, followed by HSC isolation by the combination of gradient centrifugation and vitamin A-based single cell FACS sorting. Analysis included qHSCs from untreated mice (n=58) and HSCs 6 days after TAA (n=50), 12 days after TAA (n=102), and 24 days after TAA (n=58). Following preamplification, single cell qPCR was performed for Col1a1 (left panel). Shown is one out of two representative HSC isolations per time point. Sirius Red staining demonstrates TAA-induces fibrosis induction and reversal after cessation of injury. **B.** Vim-Cre mice were treated with 18 intraperitoneal injections of TAA and tamoxifen or tamoxifen alone as indicated, followed by HSC isolation by gradient centrifugation. Expression of mGFP was determined by flow-cytometric analysis of Vitamin A-autofluorescent HSCs. Shown are representative FACS images of each time point (left panels) and quantification (right panel) of HSCs isolated from control mice (n=6), HSCs isolated 3 days (n=4) and 45 days (n=3) after the last TAA injection. C-D. Expression of mGFP was determined by fluorescent microscopy of plated HSCs isolated from TAA-treated or tamoxifen only control mice at various time points. Shown are representative pictures of vitamin A fluorescence, mGFP expression and an overlay of both (C.), and a quantification (D.) of GFP-positive/Vitamin A-positive HSCs. E. Fibrogenic gene expression in whole liver from Vim-CreER mice was performed by qPCR in TAA-treated mice at day 3 (n=4) or day 45 (n=3) after the last CCl_4 injection or in mice receiving tamoxifen only ("Ctrl", n=6). * $p<0.05$, ** $p<0.01$

Supplementary Figure 3. Shown is the construct for generation of VimCreER-transgenic mice by BAC recombineering.

Supplementary Figure 4. To determine whether endothelial cells are marked in VimCreER transgenic mice, frozen sections of CCl_4-treated liver, stomach, small intestine and colon were stained for CD31 and analyzed by confocal microscopy. All sections show close but separate localization of CD31-positive endothelium (red) and mGFP (green). Nuclei were stained by Hoechst (blue).

Supplementary Figure 5. To determine whether macrophages are marked in VimCreER transgenic mice, frozen sections of CCl_4-treated liver, stomach and colon were stained for F4/80 and analyzed by confocal microscopy. All sections show close but separate localization of F4/80-positive macrophages (red) and mGFP (green). Nuclei were stained by Hoechst (blue).

Supplementary Figure 6. Confocal microscopy of livers from either 2 week bile duct ligated mice or sham-operated mice showing Vim-CreER mediated recombination by green mGFP fluorescence, and unrecombined cells by red mTom fluorescence. Nuclei were stainted by Hoechst (blue).

Supplementary Figure 7. A-B. Mice that either did or did not receive 4 injections of CCl_4 were sacrificed 31 days after their last tamoxifen injection (corresponding to 30 days after their last CCl_4 injection). Frozen liver sections were analyzed for the percentage of mGFP-positive area in mice that received CCl_4 (n=7) or mice that did not receive CCl_4 (n=4) (A.). HSCs were isolated from mice that received CCl_4 (n=7) or mice that did not receive CCl_4 (n=3) and the percentage of GFP-positive cells among all Vitamin A-positive cells was determined by counting (B.).

Supplementary Figure 8. A. Schematic diagram showing the timing of tamoxifen and CCl_4 injections, and sacrifice at 2, and 45 days after the last CCl_4 injection of VimCreER mice. B. Sirius Red images show almost complee reversal of liver fibrosis at d45 after 8 CCl_4 injections. C. mGFP and mTom expression in livers of untreated or CCl_4-treated mice were visualized by confocal microscopy 2, and 45 days after the last CCl_4 injection or a time point corresponding to 45 days after the last CCl_4 injection in the tamoxifen only control mice. The middle and right panel show higher magnification representing the area marked by dotted white lines in the left panel. D. mGFP expression was quantified and expressed as percentage of total area for CCl_4-treated mice at day 2 (n=6) or day 45 (n=5) after the last CCl_4 injection or mice receiving tamoxifen only ("Ctrl", n=6). E. Fibrogenic gene expression in whole liver from Vim-CreER mice was performed by qPCR in CCl_4-treated mice at day 2 (n=6) or day 45 (n=5) after the last CCl_4 injection or in mice receiving tamoxifen only ("Ctrl", n=6). F-G. HSCs were isolated from CCl_4-treated mice at d2 and d45 after last CCl_4 injection or from tams. HSCs from control mice receiving corn oil and tamoxifen only were isolated at a time corresponding to 45 days after the last CCl_4 injection. Expression of mGFP was determined by flow-cytometric analysis of Vitamin A-autofluorescent HSCs. Shown are representative FACS images of each time point (F.) and quantification (G.) of HSCs isolated from untreated mice (n=3), HSCs isolated 2 days (n=2) and 45 days (n=3) after the last CCl_4 injection. Inserts show HSCs from each sorted cell population confirming cells as vitamin A-positive HSCs that either do not express mGFP and are mTom positive, or express mGFP but not mTom. H-I. Expression of mGFP was determined by fluorescent microscopy of plated HSCs isolated from CCl_4-treated or tamoxifen only control mice at various time points. Shown are representative pictures of vitamin A fluorescence, mGFP expression and an overlay of both (H.), and a quantification (I.) of GFP-positive/Vitamin A-positive HSCs. * $p<0.05$ ** $p<0.01$

Supplementary Figure 9. Wild-type mice underwent bone marrow transplantation with mTom-mGFP+/Vim-CreER+ bone marrow as described in Methods and Material followed by 4 intraperitoneal injections of CCl_4 (0.5 µl/g body weight). A. Representative images at peak fibrosis (d2) and after fibrosis resolution (d30) show abundant bone mTom-positive marrow-derived inflammatory cells but only extremely rare mGFP-positive cell. B-C. HSCs were isolated from 4xCCl_4-treated bone marrow-chimeric mice

2 and 30 days after the last CCl_4 injection. FACS analysis (B) and fluorescent microscopy (C) did not show significant presence of mGFP-positive HSCs.

Supplementary Figure 10. A-B. Display of the IPA pathway analysis for 37 genes that were altered in reverted HSCs in comparison to qHSCs fulfilling the criteria of False Discovery Rate <0.05 and $|\log_2 FC| > 0.67$. Show is the IPA analysis for gene functions (A) and canonical pathways (B) using the 37 genes with sign Supplementary Table 1.

Supplementary Table 1. Shown are the gene symbol, description, log fold change, p-value, corrected p-value ("fdr"), gene ontology biological process, gene ontology cellular component, gene ontology molecular function and pathway annotation for all 37 genes that were significantly different between reverted HSCs and qHSCs (fulfilling the criteria of False Discovery Rate <0.05 and $|\log_2 FC| > 0.67$).

Supplementary Table 2. Hepatic stellate cells were isolated from age-matched untreated mice (n=4) or mice that had undergone 4 CCl_4 injections followed by a 45 day recovery period (n=4) followed by microarray analysis using Affymetrix 1.0 ST arrays. Shown are all annoted genes with more than 0.5 log change and an uncorrected p-value of < 0.01.

Supplementary References

1. Dapito DH, Mencin A, Gwak GY, et al. Promotion of Hepatocellular Carcinoma by the Intestinal Microbiota and TLR4. Cancer Cell 2012;21:504-16.
2. Irizarry RA, Hobbs B, Collin F, et al. Exploration, normalization, and summaries of high density oligonucleotide array probe level data. Biostatistics 2003;4:249-64.
3. Smyth GK. Linear Models and Empirical Bayes Methods for Assessing Differential Expression in Microarray Experiments. Statistical Applications in Genetics and Molecular Biology 2004;3:Article 3, http://www.bepress.com/sagmb/vol3/iss1/art3/.
4. Gentleman RC, Carey VJ, Bates DM, et al. Bioconductor: open software development for computational biology and bioinformatics. Genome Biol 2004;5:R80.
5. Benjamini Y, Hochberg Y. Controlling the false discovery rate: a practical and powerful approach to multiple testing. Journal of the Royal Statistical Society 1995;57:289-300.
6. Everitt BS, Landau S, Leese M. Cluster Analysis. Arnold, 2001.
7. de Hoon MJ, Imoto S, Nolan J, et al. Open source clustering software. Bioinformatics 2004;20:1453-4.
8. Saldanha AJ. Java Treeview--extensible visualization of microarray data. Bioinformatics 2004;20:3246-8.
9. Kluwe J, Pradere JP, Gwak GY, et al. Modulation of hepatic fibrosis by c-Jun-N-terminal kinase inhibition. Gastroenterology 2010;138:347-59.
10. Seki E, De Minicis S, Osterreicher CH, et al. TLR4 enhances TGF-beta signaling and hepatic fibrosis. Nat Med 2007;13:1324-32.

Suppl. Table 1

Click here to download Supporting Document: Suppl Table1 R2 Submission June12.pdf

Symbol	Description	log_2FC	P.Value	fdr	GO_biological_process	GO_cellular_component	GO_molecular_function	pathway
Lgi2	leucine-rich repeat LGI family, member 2	-1.27	9.94E-07	0.009	---	extracellular region	protein binding	---
Cacna1c	calcium channel, voltage-dependent, L type, alpha 1C subunit	-1.17	1.66E-06	0.009	transport ion transport calcium ion transport cellular calcium ion homeostasis smooth muscle contraction synaptic transmission adult walking behavior regulation of blood pressure visual learning calcium ion-dependent exocytosis regulation of vasoconstriction insulin secretion growth hormone secretion glucose homeostasis regulation of organ growth transmembrane transport smooth muscle contraction involved in micturition	caveolar macromolecular signaling complex assay membrane fraction plasma membrane voltage-gated calcium channel complex membrane integral to membrane Z disc T-tubule sarcolemma neuronal cell body dendritic shaft	osteoblast differentiation eye developmen kidney development endochondral ossification inflammatory response multicellular organismal development cell differentiation BMP signaling pathway male genitalia development growth positive regulation of neuron differentiation positive regulation of osteoblast differentiation cartilage development	Calcium_regulation_in_cardiac_cells
Bmp6	bone morphogenetic protein 6	-0.92	1.95E-06	0.009	---	extracellular region extracellular space cytoplasm membrane-bounded vesicle	cytokine activity protein binding growth factor activity protein heterodimerization activity BMP receptor binding	---
Svep1	sushi, von Willebrand factor type A, EGF and pentraxin domain containing 1	-1.30	1.96E-06	0.009	cell adhesion	extracellular region cytoplasm membrane extracellular region	chromatin binding calcium ion binding protein binding	---
Gpr126	G protein-coupled receptor 126	-1.04	2.16E-06	0.009	signal transduction; cell surface receptor linked signaling pathway; G-protein coupled receptor protein signaling pathway; neuropeptide signaling pathway	cytoplasm plasma membrane cell surface membrane integral to membrane	signal transducer activity receptor activity transmembrane receptor activity G-protein coupled receptor activity	---
Cyp1b1	cytochrome P450, family 1, subfamily b, polypeptide 1	-0.85	2.19E-06	0.009	cellular aromatic compound metabolic process estrogen metabolic process toxin metabolic process dibenzo-p-dioxin metabolic process oxidation reduction	endoplasmic reticulum microsome	monooxygenase activity iron ion binding electron carrier activity oxidoreductase activity heme binding metal ion binding aromatase activity monooxygenase activity	---
Sectm1a	secreted and transmembrane 1A	1.27	2.70E-06	0.010	---	extracellular region plasma membrane membrane integral to membrane	---	---
Ano4	anoctamin 4	-1.02	3.62E-06	0.011	transport ion transport	membrane integral to membrane chloride channel complex	ion channel activity chloride channel activity	---
Il2rg	interleukin 2 receptor, gamma chain	-0.89	3.67E-06	0.011	positive regulation of CD4-positive, CD25-positive, alpha-beta regulatory T cell differentiation positive regulation of T cell differentiation in the thymi positive regulation of B cell differentiation	external side of plasma membrane cell surface integral to membrane	receptor activity cytokine receptor activity interleukin-2 binding interleukin-7 binding	Inflammatory_Response_Pathway
Cxcl14	chemokine (C-X-C motif) ligand 14	-1.08	5.38E-06	0.013	immune response	extracellular region extracellular space	cytokine activity chemokine activity	---
Clic5	chloride intracellular channel 5	-1.32	6.19E-06	0.013	transport ion transport chloride transport sensory perception of sound protein localization neuromuscular process controlling balance auditory receptor cell stereocilium organization ilium organization	cytoplasm Golgi apparatus cytoskeleton membrane integral to membrane stereocilium chloride channel complex	ion channel activity voltage-gated ion channel activity voltage-gated chloride channel activity chloride channel activity	---
Fam19a1	family with sequence similarity 19, member A1	1.02	7.08E-06	0.013	---	extracellular region	---	---
Nufip1	nuclear fragile X mental retardation protein interacting protein 1	-0.73	9.21E-06	0.014	positive regulation of transcription from RNA polymer	nucleus perichromatin fibrils nucleolus transcription elongation factor complex nuclear matrix cytosolic ribosome presynaptic active zone	RNA binding protein binding zinc ion binding metal ion binding	mRNA_processing_binding
Myo1d	myosin !D	-1.06	1.67E-06	0.009	negative regulation of phosphatase activity	myosin complex	ATP binding actin binding calmodulin binding	---
Lox	lysyl oxidase	-1.05	1.54E-05	0.019	blood vessel development response to hormone stimulus collagen fibril organization lung development wound healing elastic fiber assembly oxidation reduction	extracellular region proteinaceous extracellular matrix collagen	protein-lysine 6-oxidase activity copper ion binding oxidoreductase activity oxidoreductase activity, acting on the CH-NH2 group of donors, oxygen as acceptor metal ion binding	---
Tmem10ε	transmembrane protein 108	-1.25	1.55E-05	0.019	---	membrane integral to membrane	---	---
Csprs	component of Sp100-rs	-0.89	1.73E-05	0.020	---	nucleus	N receptor activity	---
Gm7609	predicted gene 7609	-1.02	1.78E-05	0.020	---	nucleus	receptor activity	---

Enpep	glutamyl aminopeptidase	-1.27	1.86E-05	0.020	angiogenesis cell migration proteolysis cell proliferation	plasma membrane brush border membrane integral to membrane apical plasma membrane cytoplasmic vesicle apical part of cell	aminopeptidase activity peptidase activity zinc ion binding hydrolase activity metal ion binding	---
Hs6st3	heparan sulfate 6-O-sulfotransferase 3	0.70	2.60E-05	0.026	carbohydrate biosynthetic process	membrane integral to membrane	sulfotransferase activity	---
Wt1	Wilms tumor 1 homolog	-1.39	2.78E-05	0.027	negative regulation of transcription from RNA polymer vasculogenesis metanephros development ureteric bud development branching involved in ureteric bud morphogenesis kidney development mesonephros development transcription regulation of transcription, DNA-dependent regulation of transcription from RNA polymerase II promoter germ cell development heart development sex determination RNA splicing male gonad develop negative regulation of transcription adrenal gland development male genitalia development epithelial cell differentiation glomerulus development inferred from mutant phenotype camera-type eye development negative regulation of apoptosis regulation of transcription	intracellular cytoplasm nucleus nuclear speck	nucleic acid binding DNA binding double-stranded DNA binding transcription factor activity RNA binding protein binding zinc ion binding transcription activator activity transcription repressor activity specific transcriptional repressor activity sequence-specific DNA binding metal ion binding C2H2 zinc finger domain binding	---
Cyp7b1	cytochrome P450, family 7, subfamily b, polypeptide 1	-1.58	3.06E-05	0.028	lipid metabolic process bile acid biosynthetic process digestion memory circadian rhythm steroid metabolic process cholesterol metabolic process negative regulation of estrogen receptor signaling pathway positive regulation of epithelial cell proliferation oxidation reduction prostate gland epithelium morphogenesis	endoplasmic reticulum microsome membrane	monooxygenase activity iron ion binding oxysterol 7-alpha-hydroxylase activity electron carrier activity oxidoreductase activity heme binding 25-hydroxycholesterol 7alpha-hydroxylase activity metal ion binding	---
Abcb11	ATP-binding cassette, sub-family B (MDR	-0.77	3.09E-05	0.028	transport canalicular bile acid transport response to drug drug export transmembrane transport	Golgi membrane membrane fraction Golgi apparatus membrane integral to membrane apical plasma membrane intercellular canaliculus	nucleotide binding protein binding ATP binding canalicular bile acid transmembrane transporter activity drug transmembrane transporter activity ATPase activity nucleoside-triphosphatase activity ATPase activity, coupled to transmembrane movement of substances	---
Serpina3r	serine (or cysteine) peptidase inhibitor, clade A, member 3N	-1.03	3.24E-05	0.028	acute-phase response response to cytokine stimulus response to peptide hormone stimulus	cell fraction extracellular region	serine-type endopeptidase inhibitor activity peptidase inhibitor activity	---
Gda	guanine deaminase	-0.68	3.48E-05	0.029	---	---	protein binding zinc ion binding guanine deaminase activity hydrolase activity metal ion binding	---
Frmd4b	FERM domain containing 4B	-0.72	3.96E-05	0.029	---	cytoplasm cytoskeleton	---	---
LOC6333	similar to dachsous 2 isoform 2	0.75	4.22E-05	0.029	---	---	---	---
Neto1	neuropilin (NRP) and tolloid (TLL)-like 1	0.87	4.35E-05	0.029	memory visual learning regulation of long-term neuronal synaptic plasticit	plasma membrane postsynaptic density membrane integral to membrane cell junction synapse postsynaptic membrane excitatory synapse	receptor activity protein binding	---
Serpini1	serine (or cysteine) peptidase inhibitor, clade I, member 1	-0.91	4.38E-05	0.029	regulation of cell adhesion	extracellular region	serine-type endopeptidase inhibitor activity peptidase inhibitor activity	---
Thbs1	thrombospondin 1	-1.00	4.54E-05	0.029	growth plate cartilage development inflammatory response cell adhesion positive regulation of cell-substrate adhesion negative regulation of angiogenesis	extracellular region extracellular space	structural molecule activity calcium ion binding protein binding extracellular matrix binding	TGF_Beta_Signaling_Pathway
Pcdh15	protocadherin 15	0.81	4.71E-05	0.029	startle response morphogenesis of an epithelium actin filament organization cell adhesion homophilic cell adhesion visual perception	membrane integral to membrane stereocilium photoreceptor outer segment cytoplasm	calcium ion binding protein binding	---

					sensory perception of sound locomotory behavior adult walking behavior adult locomotory behavior sensory cilium assembly multicellular organism growth auditory receptor cell differentiation inner ear development response to stimulus detection of mechanical stimulus involved in sensory perception of sound detection of mechanical stimulus involved in equilibrioception righting reflex auditory receptor cell stereocilium organization auditory receptor cell stereocilium			
Olfml2b	olfactomedin-like 2B	-0.75	4.86E-05	0.029	extracellular matrix organization	extracellular region membrane extracellular matrix	protein homodimerization activity extracellular matrix binding	---
Epha3	Eph receptor A3	-0.89	6.22E-05	0.036	protein amino acid phosphorylation transmembrane receptor protein tyrosine kinase signa	extracellular region plasma membrane integral to plasma membrane membrane integral to membrane	nucleotide binding protein kinase activity protein tyrosine kinase activity transmembrane receptor protein tyrosine kinase activity receptor activity ephrin receptor activity protein binding ATP binding kinase activity transferase activity	---
Elovl6	ELOVL family member 6, elongation of long chain fatty acids (yeast)	-0.96	7.01E-05	0.038	fatty acid biosynthetic process lipid biosynthetic process fatty acid elongation	mitochondrion endoplasmic reticulum membrane integral to membrane integral to endoplasmic reticulum membrane	transferase activity, transferring acyl groups o	---
Gcnt2	glucosaminyl (N-acetyl) transferase 2, I-branching enzyme	-0.68	7.66E-05	0.041	---	Golgi apparatus membrane integral to membrane	N-acetyllactosaminide beta-1,6-N-acetylglucos acetylglucosaminyltransferase activity transferase activity transferase activity, transferring glycosyl groups	---
Ace2	angiotensin I converting enzyme (peptidyl-dipeptidase A) 2	-1.93	8.37E-05	0.044	proteolysis	extracellular region membrane fraction plasma membrane membrane integral to membrane	carboxypeptidase activity peptidase activity metallopeptidase activity peptidyl-dipeptidase activity hydrolase activity peptide hormone binding peptide binding	---
Sema5a	sema domain, seven thrombospondin repeats (type 1 and type 1-like), transmembrane domain (TM) and short cytoplasmic domain, (semaphorin) 5A	-0.80	0.00011	0.049	patterning of blood vessels multicellular organismal development nervous system development axon guidance cell differentiation branching morphogenesis of a tube	membrane integral to membrane	receptor activity axon guidance receptor activity	---

Suppl. Table 2

Click here to download Supporting Document: Suppl Table 2 R2 Submission June 13.pdf

probe	Symbol	Description	logFC (reverted HSC vs qHSC)	P.Value	adj.P.Val
10376201	Gpx3	glutathione peroxidase 3	1.972522813	0.00012622	0.05205665
10603066	Ace2	angiotensin I converting enzyme (peptidyl-dipeptidase A)	1.927354318	8.37E-05	0.04439331
10358389	Rgs2	regulator of G-protein signaling 2	1.837423785	0.0008682	0.13191724
10351293	Dpt	dermatopontin	1.692504125	0.00014251	0.05422964
10497381	Cyp7b1	cytochrome P450, family 7, subfamily b, polypeptide 1	1.581680526	3.06E-05	0.02816903
10346882	Adam23	a disintegrin and metallopeptidase domain 23	1.40256214	0.00100028	0.13838858
10474295	Wt1	Wilms tumor 1 homolog	1.388894992	2.78E-05	0.02745547
10445347	Clic5	chloride intracellular channel 5	1.320841573	6.19E-06	0.01322506
10513208	Svep1	sushi, von Willebrand factor type A, EGF and pentraxin do	1.304258041	1.96E-06	0.00865815
10530029	Lgi2	leucine-rich repeat LGI family, member 2	1.273740262	9.94E-07	0.00865815
10502081	Enpep	glutamyl aminopeptidase	1.273279293	1.86E-05	0.02000148
10523175	Ereg	epiregulin	1.270140957	0.00030251	0.07900051
10596200	Tmem108	transmembrane protein 108	1.252323336	1.55E-05	0.01921247
10354247	Fhl2	four and a half LIM domains 2	1.196017233	0.00019615	0.06518024
10547322	Cacna1c	calcium channel, voltage-dependent, L type, alpha 1C sub	1.170848106	1.66E-06	0.00865815
10545588	Hk2	hexokinase 2	1.104627815	0.00107386	0.1413395
10409579	Cxcl14	chemokine (C-X-C motif) ligand 14	1.077666665	5.38E-06	0.01274644
10389022	Myo1d	myosin ID	1.058509366	1.67E-06	0.00865815
10458894	Lox	lysyl oxidase	1.051891849	1.54E-05	0.01921247
10367982	Gpr126	G protein-coupled receptor 126	1.037333014	2.16E-06	0.00865815
10398075	Serpina3n	serine (or cysteine) peptidase inhibitor, clade A, member	1.031793537	3.24E-05	0.02819706
10389025	Myo1d	myosin ID	1.021271541	1.16E-05	0.0158523
10519140	Mmp23	matrix metallopeptidase 23	1.021208459	0.00016005	0.05662672
10347915	Gm7609	predicted gene 7609	1.017141954	1.78E-05	0.0198244
10371740	Ano4	anoctamin 4	1.015441666	3.62E-06	0.01086987
10474700	Thbs1	thrombospondin 1	1.004864322	4.54E-05	0.02868669
10514576	Kank4	KN motif and ankyrin repeat domains 4	1.003024026	0.00299599	0.20263964
10379190	Vtn	vitronectin	0.971515522	0.00046312	0.09919756
10495993	Elovl6	ELOVL family member 6, elongation of long chain fatty ac	0.961534165	7.01E-05	0.03845938
10347925	Gm7609	predicted gene 7609	0.930000336	2.92E-05	0.02801806
10472050	Tnfaip6	tumor necrosis factor alpha induced protein 6	0.926995164	0.00302889	0.20263964
10404686	Bmp6	bone morphogenetic protein 6	0.915266697	1.95E-06	0.00865815
10492628	Serpini1	serine (or cysteine) peptidase inhibitor, clade I, member :	0.913461887	4.38E-05	0.02868669
10492682	Fam198b	family with sequence similarity 198, member B	0.894280878	0.00177647	0.17445586
10606016	Il2rg	interleukin 2 receptor, gamma chain	0.890401451	3.67E-06	0.01086987
10582879	Csprs	component of Sp100-rs	0.888149241	1.73E-05	0.0198244
10440258	Epha3	Eph receptor A3	0.887090876	6.22E-05	0.03568256
10498273	Tm4sf1	transmembrane 4 superfamily member 1	0.874013407	0.00024545	0.0707632
10543939	Fam180a	family with sequence similarity 180, member A	0.871269849	0.00160129	0.16732915
10356274	Csprs	component of Sp100-rs	0.868319055	4.80E-06	0.01218651
10577164	Gas6	growth arrest specific 6	0.8561532	0.00016404	0.05662672
10453057	Cyp1b1	cytochrome P450, family 1, subfamily b, polypeptide 1	0.850680766	2.19E-06	0.00865815
10409278	Nfil3	nuclear factor, interleukin 3, regulated	0.848662199	0.00260755	0.19684377
10398665	Tnfaip2	tumor necrosis factor, alpha-induced protein 2	0.829606141	0.00107587	0.1413395
10513739	Tnc	tenascin C	0.802872452	0.00022166	0.06954526
10581605	Hp	haptoglobin	0.801193397	0.00045381	0.09899118
10570855	Plat	plasminogen activator, tissue	0.800964667	0.00624244	0.23798162
10423520	Sema5a	sema domain, seven thrombospondin repeats (type 1 and	0.795883749	0.00010765	0.04906987
10452316	C3	complement component 3	0.77933108	0.0092851	0.26145665
10431051	Scube1	signal peptide, CUB domain, EGF-like 1	0.777266301	0.00437326	0.21724195
10416340	Gfra2	glial cell line derived neurotrophic factor family receptor a	0.77238485	0.0007241	0.12153893
10483410	Abcb11	ATP-binding cassette, sub-family B (MDR	0.771363578	3.09E-05	0.02816903
10518947	Ajap1	adherens junction associated protein 1	0.762066761	0.00145582	0.15976247
10354598	Hecw2	HECT, C2 and WW domain containing E3 ubiquitin protein	0.760229164	0.00029718	0.07826996
10566583	Gm8995	predicted gene 8995	0.758221323	0.0001295	0.05205665
10351491	Olfml2b	olfactomedin-like 2B	0.748412221	4.86E-05	0.02878946
10583870	Bmper	BMP-binding endothelial regulator	0.732885083	0.00066255	0.11778829
10416510	Nufip1	nuclear fragile X mental retardation protein interacting pr	0.725900868	9.21E-06	0.01363897
10567010	Dkk3	dickkopf homolog 3 (Xenopus laevis)	0.724522083	0.00750015	0.25096337
10546631	Frmd4b	FERM domain containing 4B	0.721477602	3.96E-05	0.02868669
10449775	Notch3	Notch gene homolog 3 (Drosophila)	0.714949644	0.00448491	0.21924316
10349401	Gpr39	G protein-coupled receptor 39	0.714494964	0.00045928	0.09919756
10360920	Tgfb2	transforming growth factor, beta 2	0.70396054	0.00498294	0.22541125
10424400	Myc	myelocytomatosis oncogene	0.696201959	0.00195474	0.1786704
10450242	C4b	complement component 4B (Childo blood group)	0.6958992	0.00645342	0.23976783
10359851	Uck2	uridine-cytidine kinase 2	0.686426469	0.00078294	0.12516412
10447120	Tmem178	transmembrane protein 178	0.679304549	0.00181126	0.17595902
10591988	Adamts15	a disintegrin-like and metallopeptidase (reprolysin type) v	0.677325308	0.00913104	0.26136208
10466659	Gda	guanine deaminase	0.676418111	3.48E-05	0.02868669
10404702	Gcnt2	glucosaminyl (N-acetyl) transferase 2, I-branching enzym	0.675495726	7.66E-05	0.04125593
10528008	Steap2	six transmembrane epithelial antigen of prostate 2	0.666933779	0.00014881	0.05516465
10515201	Cyp4b1	cytochrome P450, family 4, subfamily b, polypeptide 1	0.662634103	0.00025922	0.07257302
10344897	Sulf1	sulfatase 1	0.661236795	0.00012844	0.05205665
10587799	Plscr2	phospholipid scramblase 2	0.649720785	0.00404369	0.21724195
10443527	Pim1	proviral integration site 1	0.644888464	0.00295902	0.20263964
10592061	Kcnj5	potassium inwardly-rectifying channel, subfamily J, memt	0.640025215	0.00229079	0.18848973
10471844	Nek6	NIMA (never in mitosis gene a)-related expressed kinase	0.624610531	1.02E-05	0.01445043
10598976	Timp1	tissue inhibitor of metalloproteinase 1	0.624453328	0.00696627	0.24379217
10358434	Pla2g4a	phospholipase A2, group IVA (cytosolic, calcium-dependei	0.612092619	0.00193664	0.1786704

10553477	Ano5	anoctamin 5	0.607171723	6.36E-06	0.01322506
10542355	Emp1	epithelial membrane protein 1	0.604904499	0.00068817	0.12049468
10510215	Gm13139	predicted gene 13139	0.603143378	0.00477605	0.22270434
10427436	C7	complement component 7	0.60207043	0.00547479	0.23036896
10509965	Epha2	Eph receptor A2	0.601855076	0.00652102	0.24063318
10352905	Cd34	CD34 antigen	0.599524327	0.00128869	0.151724
10446928	Ltbp1	latent transforming growth factor beta binding protein 1	0.596753589	9.33E-05	0.04609884
10483228	Scn3a	sodium channel, voltage-gated, type III, alpha	0.588968202	0.00577827	0.23233878
10372648	Lyz2	lysozyme 2	0.588634127	0.00549663	0.23046935
10485405	Cd44	CD44 antigen	0.587075316	0.00037232	0.08944678
10369842	Bicc1	bicaudal C homolog 1 (Drosophila)	0.585781156	1.70E-05	0.0198244
10505996	Fggy	FGGY carbohydrate kinase domain containing	0.585065639	0.0015667	0.1662848
10512372	Ccl19	chemokine (C-C motif) ligand 19	0.579624058	8.07E-06	0.01322506
10601456	Gm6377	predicted gene 6377	0.579243547	0.00895766	0.25957966
10537062	Mest	mesoderm specific transcript	0.578485257	3.40E-05	0.02868669
10532741	Tmem119	transmembrane protein 119	0.578004	0.00078994	0.12538904
10366546	Cpm	carboxypeptidase M	0.574049514	0.00954029	0.26188924
10504159	Ccl19	chemokine (C-C motif) ligand 19	0.570114247	8.55E-06	0.01322506
10512322	Ccl19	chemokine (C-C motif) ligand 19	0.570114247	8.55E-06	0.01322506
10522288	Shisa3	shisa homolog 3 (Xenopus laevis)	0.567717348	0.00064558	0.11702634
10375614	Gfpt2	glutamine fructose-6-phosphate transaminase 2	0.566388764	0.00871706	0.25799458
10365290	Chst11	carbohydrate sulfotransferase 11	0.56435666	0.00012109	0.0519067
10504188	Ccl19	chemokine (C-C motif) ligand 19	0.558764469	7.61E-06	0.01322506
10357833	Atp2b4	ATPase, Ca++ transporting, plasma membrane 4	0.558001403	0.00022298	0.06954526
10360764	Enah	enabled homolog (Drosophila)	0.556954833	0.00087735	0.13192692
10440091	Col8a1	collagen, type VIII, alpha 1	0.553670281	0.00266385	0.19815026
10506201	Ror1	receptor tyrosine kinase-like orphan receptor 1	0.552640345	2.09E-06	0.00865815
10367634	Akap12	A kinase (PRKA) anchor protein (gravin) 12	0.549861371	0.00254164	0.19684377
10428534	Trps1	trichorhinophalangeal syndrome I (human)	0.548859349	0.00202658	0.17904196
10406452	Gm10759	predicted gene 10759	0.545255996	0.00508263	0.22584067
10366293	Csrp2	cysteine and glycine-rich protein 2	0.544808126	0.00019816	0.06523992
10381387	G6pc	glucose-6-phosphatase, catalytic	0.544493465	0.00860248	0.25799458
10583732	Ldlr	low density lipoprotein receptor	0.537354906	0.0061269	0.23636104
10469066	Ccdc3	coiled-coil domain containing 3	0.531261645	6.81E-05	0.03845938
10504132	Ccl19	chemokine (C-C motif) ligand 19	0.527855836	4.74E-06	0.01218651
10406434	Mef2c	myocyte enhancer factor 2C	0.521596317	1.57E-05	0.01921247
10368409	Lama2	laminin, alpha 2	0.520440474	0.00028383	0.07607355
10541246	Il17ra	interleukin 17 receptor A	0.515519815	0.00024586	0.0707632
10424404	Pvt1	plasmacytoma variant translocation 1	0.509319269	0.00496439	0.22514604
10543802	Plxna4	plexin A4	0.508445877	0.00939374	0.26163688
10405211	Gadd45g	growth arrest and DNA-damage-inducible 45 gamma	0.507490172	0.00088436	0.13192692
10499655	Il6ra	interleukin 6 receptor, alpha	0.506701824	9.56E-05	0.04609884
10422728	Dab2	disabled homolog 2 (Drosophila)	0.504774144	0.00082768	0.12795141
10576774	Clec4g	C-type lectin domain family 4, member g	0.503288131	0.00125394	0.15016606
10382802	Sphk1	sphingosine kinase 1	0.502184732	0.00962681	0.26189038
10452295	Tubb4	tubulin, beta 4	0.501556379	0.00460795	0.22021561
10565456	Prss23	protease, serine, 23	0.500212102	0.00012292	0.05203145
10371466	Syn3	synapsin III	-0.500203847	0.00021168	0.06842204
10350438	Kcnt2	potassium channel, subfamily T, member 2	-0.508431044	0.00226328	0.1872908
10361926	Map3k5	mitogen-activated protein kinase kinase kinase 5	-0.509702243	0.00098055	0.13808707
10511333	Plag1	pleiomorphic adenoma gene 1	-0.513565885	0.00258524	0.19684377
10592420	AW551984	expressed sequence AW551984	-0.516453293	0.00606227	0.23636104
10596222	Ccrl1	chemokine (C-C motif) receptor-like 1	-0.548916359	0.0002154	0.06871583
10512279	Cntfr	ciliary neurotrophic factor receptor	-0.557273969	0.00057114	0.11269893
10560618	Apoc1	apolipoprotein C-I	-0.559699587	0.00246429	0.19471189
10416057	Clu	clusterin	-0.563716164	0.00059663	0.11344213
10488378	Thbd	thrombomodulin	-0.56842842	0.00051217	0.1052642
10446739	Clip4	CAP-GLY domain containing linker protein family, membe	-0.573536541	0.0026825	0.19855988
10521616	C1qtnf7	C1q and tumor necrosis factor related protein 7	-0.58469345	0.00106647	0.1413395
10497203	Hey1	hairy	-0.592042669	0.00026921	0.07478129
10471721	Ptgs1	prostaglandin-endoperoxide synthase 1	-0.601084311	0.00040191	0.09281374
10477169	Id1	inhibitor of DNA binding 1	-0.614302692	0.00327267	0.20503078
10392522	Abca8a	ATP-binding cassette, sub-family A (ABC1), member 8a	-0.614538792	0.00012777	0.05205665
10459671	Dcc	deleted in colorectal carcinoma	-0.651731019	9.79E-05	0.04609884
10390691	Nr1d1	nuclear receptor subfamily 1, group D, member 1	-0.681358255	0.00201072	0.17904196
10417048	Hs6st3	heparan sulfate 6-O-sulfotransferase 3	-0.696850191	2.60E-05	0.02640076
10492774	LOC633371	similar to dachsous 2 isoform 2	-0.74751168	4.22E-05	0.02868669
10474958	Dll4	delta-like 4 (Drosophila)	-0.748841629	0.00882764	0.25828726
10411274	Sv2c	synaptic vesicle glycoprotein 2c	-0.805564103	0.00543474	0.22949851
10482814	Acvr1c	activin A receptor, type IC	-0.807000168	0.00661379	0.24094256
10363921	Pcdh15	protocadherin 15	-0.810139002	4.71E-05	0.02878946
10490491	Gata5	GATA binding protein 5	-0.825755896	0.0003044	0.07900051
10489305	Ptprt	protein tyrosine phosphatase, receptor type, T	-0.868100163	0.00016216	0.05662672
10457091	Neto1	neuropilin (NRP) and tolloid (TLL)-like 1	-0.868690269	4.35E-05	0.02868669
10529264	Spon2	spondin 2, extracellular matrix protein	-0.904942078	0.00611255	0.23636104
10463875	Sorcs3	sortilin-related VPS10 domain containing receptor 3	-0.992107266	0.00032223	0.08225104
10540233	Fam19a1	family with sequence similarity 19, member A1	-1.016519005	7.08E-06	0.01322506
10394068	Sectm1a	secreted and transmembrane 1A	-1.266724847	2.70E-06	0.00961536

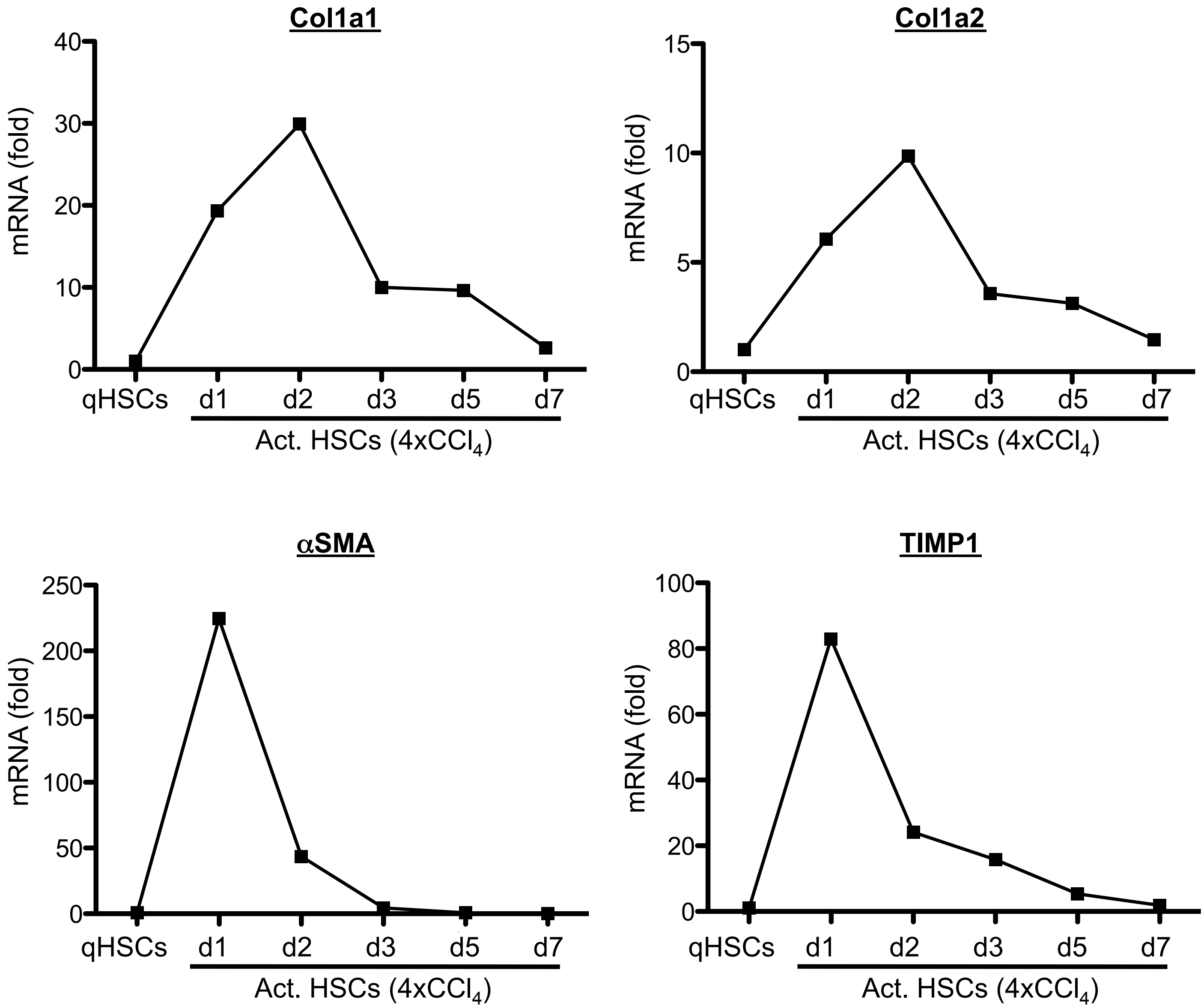
Col1a1
Col1a2
αSMA
TIMP1
mRNA (fold)
qHSCs
d1
d2
d3
d5
d7
Act. HSCs (4xCCl4)

Suppl. Fig.1

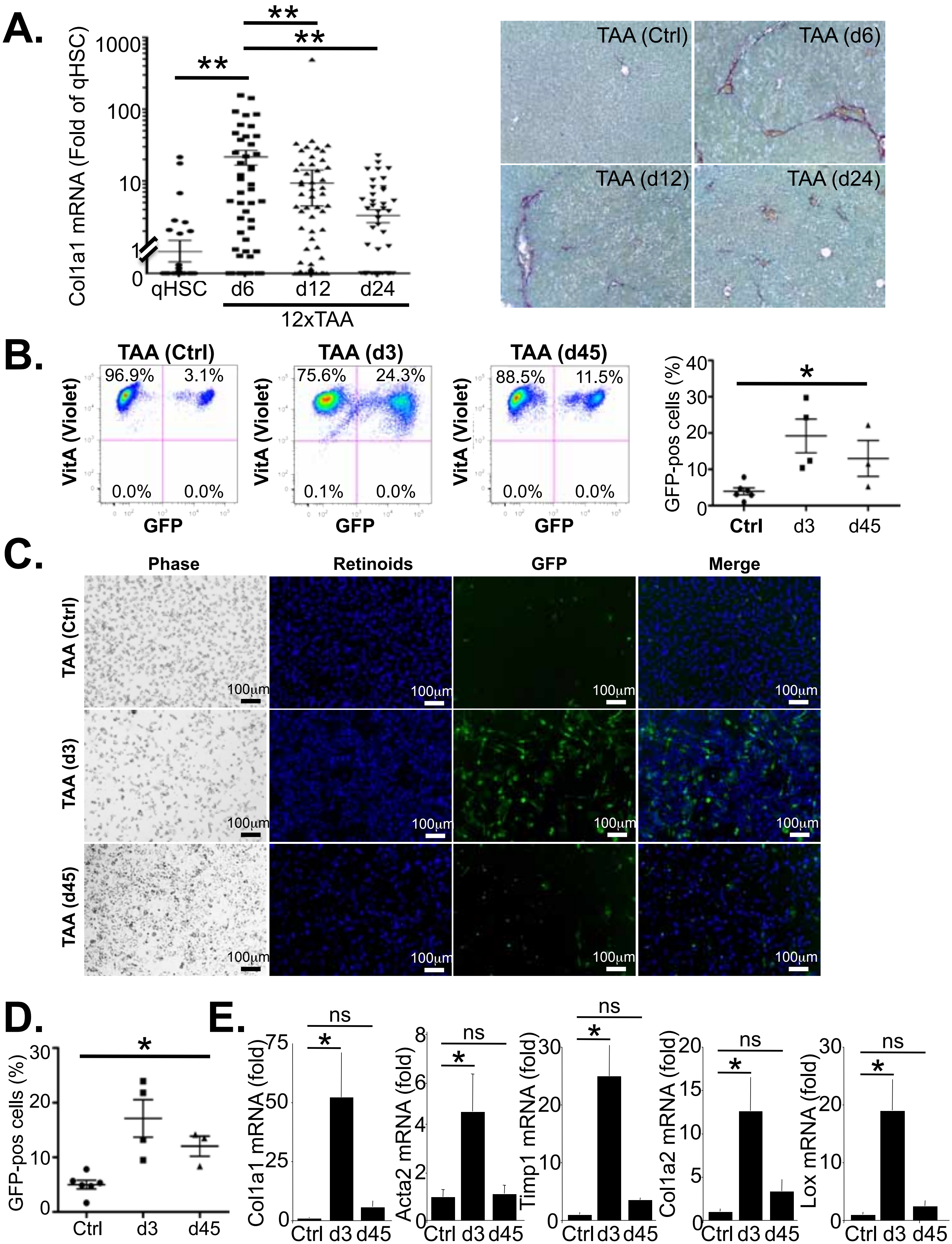
A.
Col1a1 mRNA (Fold of qHSC)
1000
100
10
1
0
**
**
**
qHSC
d6
d12
d24
12xTAA
TAA (Ctrl)
TAA (d6)
TAA (d12)
TAA (d24)
B.
TAA (Ctrl)
96.9%
3.1%
0.0%
0.0%
TAA (d3)
75.6%
24.3%
0.1%
0.0%
TAA (d45)
88.5%
11.5%
0.0%
0.0%
VitA (Violet)
GFP
GFP-pos cells (%)
40
30
20
10
0
*
Ctrl
d3
d45
C.
Phase
Retinoids
GFP
Merge
TAA (Ctrl)
TAA (d3)
TAA (d45)
100µm
D.
GFP-pos cells (%)
30
20
10
0
*
Ctrl
d3
d45
E.
Col1a1 mRNA (fold)
Acta2 mRNA (fold)
Timp1 mRNA (fold)
Col1a2 mRNA (fold)
Lox mRNA (fold)
ns
*
Ctrl
d3
d45

Suppl. Fig.2

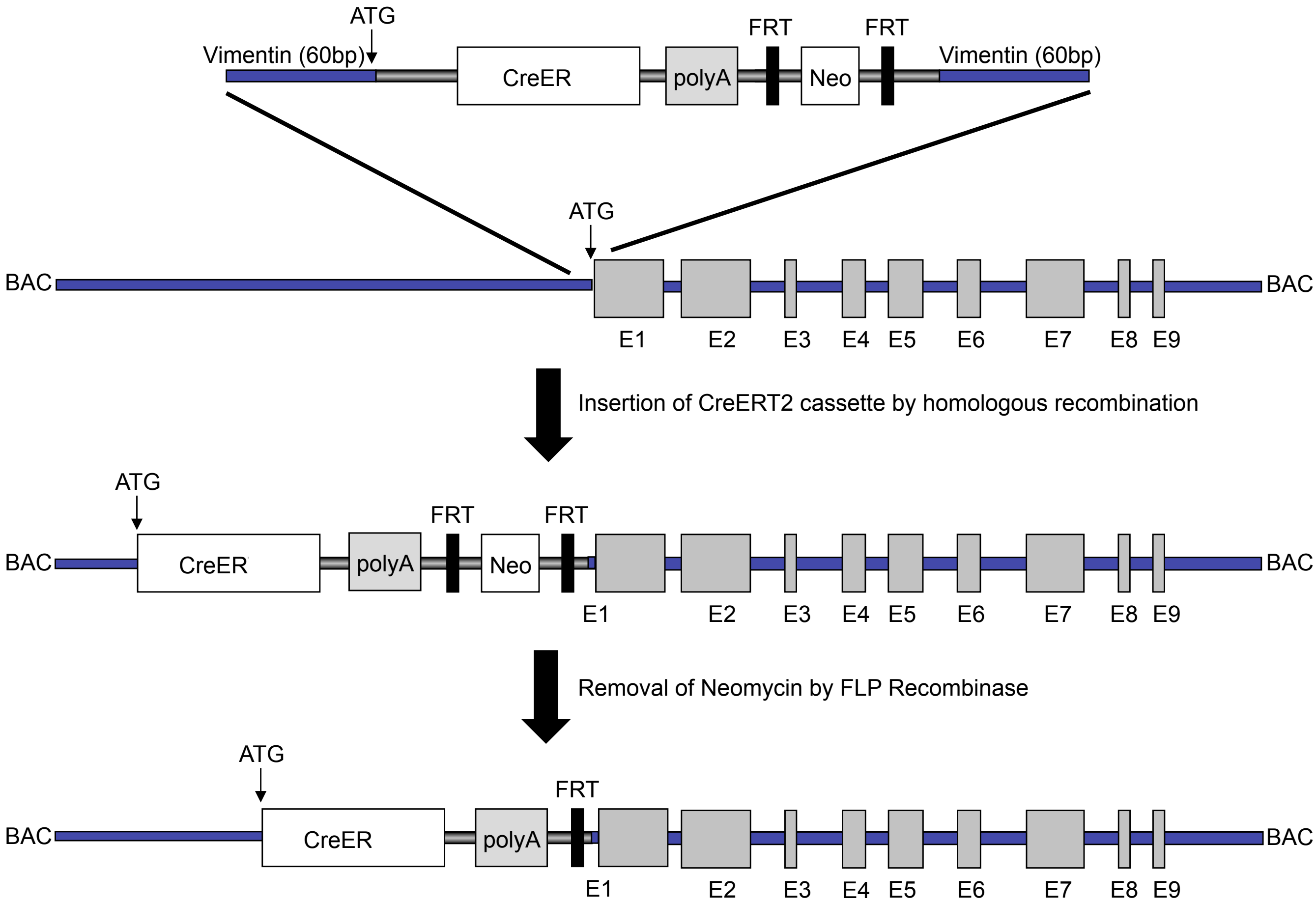
ATG
Vimentin (60bp)
CreER
polyA
FRT
Neo
FRT
Vimentin (60bp)
ATG
BAC
BAC
E1
E2
E3
E4
E5
E6
E7
E8
E9
Insertion of CreERT2 cassette by homologous recombination
ATG
BAC
CreER
polyA
FRT
Neo
FRT
BAC
E1
E2
E3
E4
E5
E6
E7
E8
E9
Removal of Neomycin by FLP Recombinase
ATG
BAC
CreER
polyA
FRT
BAC
E1
E2
E3
E4
E5
E6
E7
E8
E9

Suppl. Fig.3

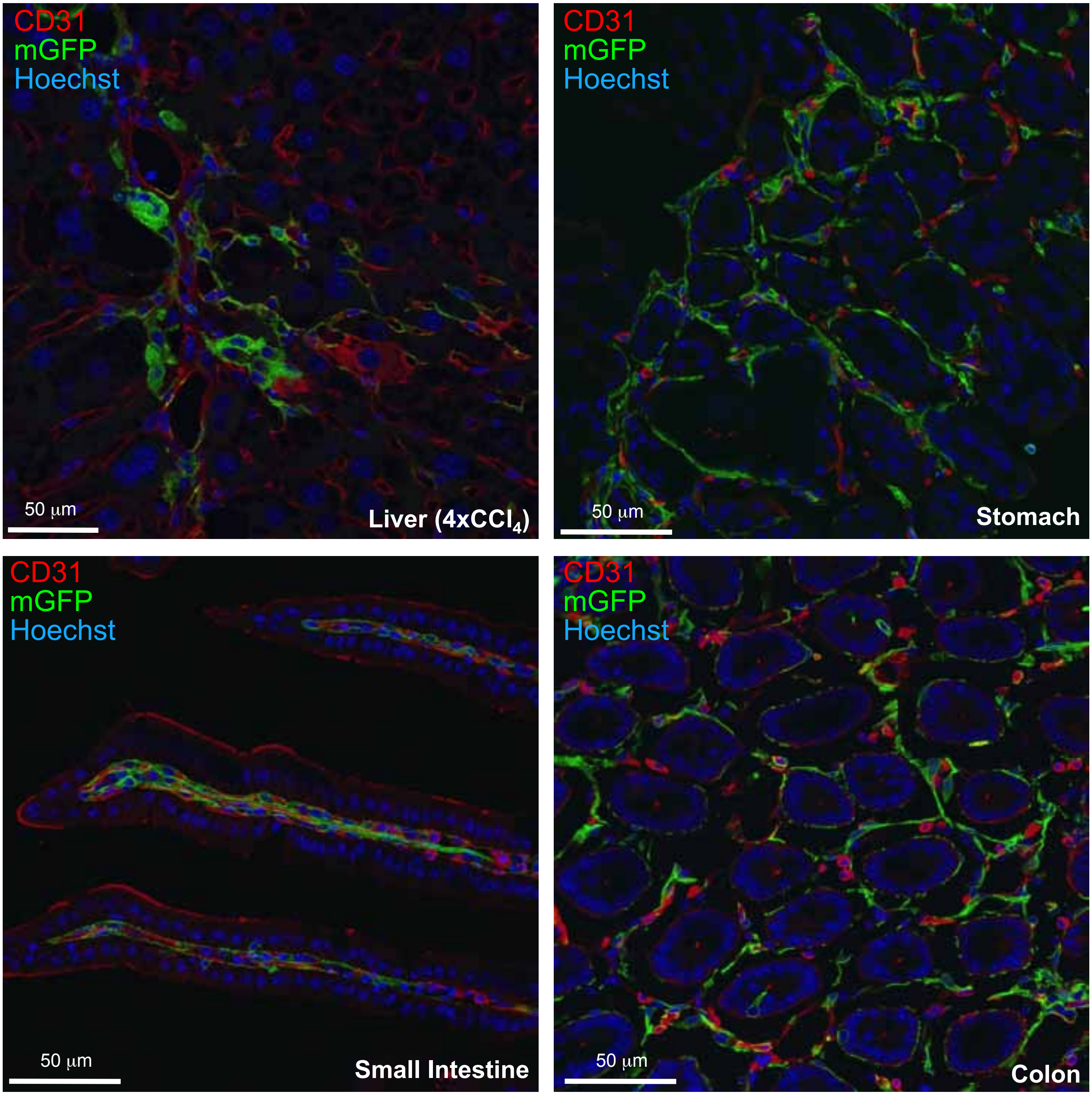

CD31
mGFP
Hoechst
50 μm
Liver (4xCCl4)
CD31
mGFP
Hoechst
50 μm
Stomach
CD31
mGFP
Hoechst
50 μm
Small Intestine
CD31
mGFP
Hoechst
50 μm
Colon

Suppl. Fig.4

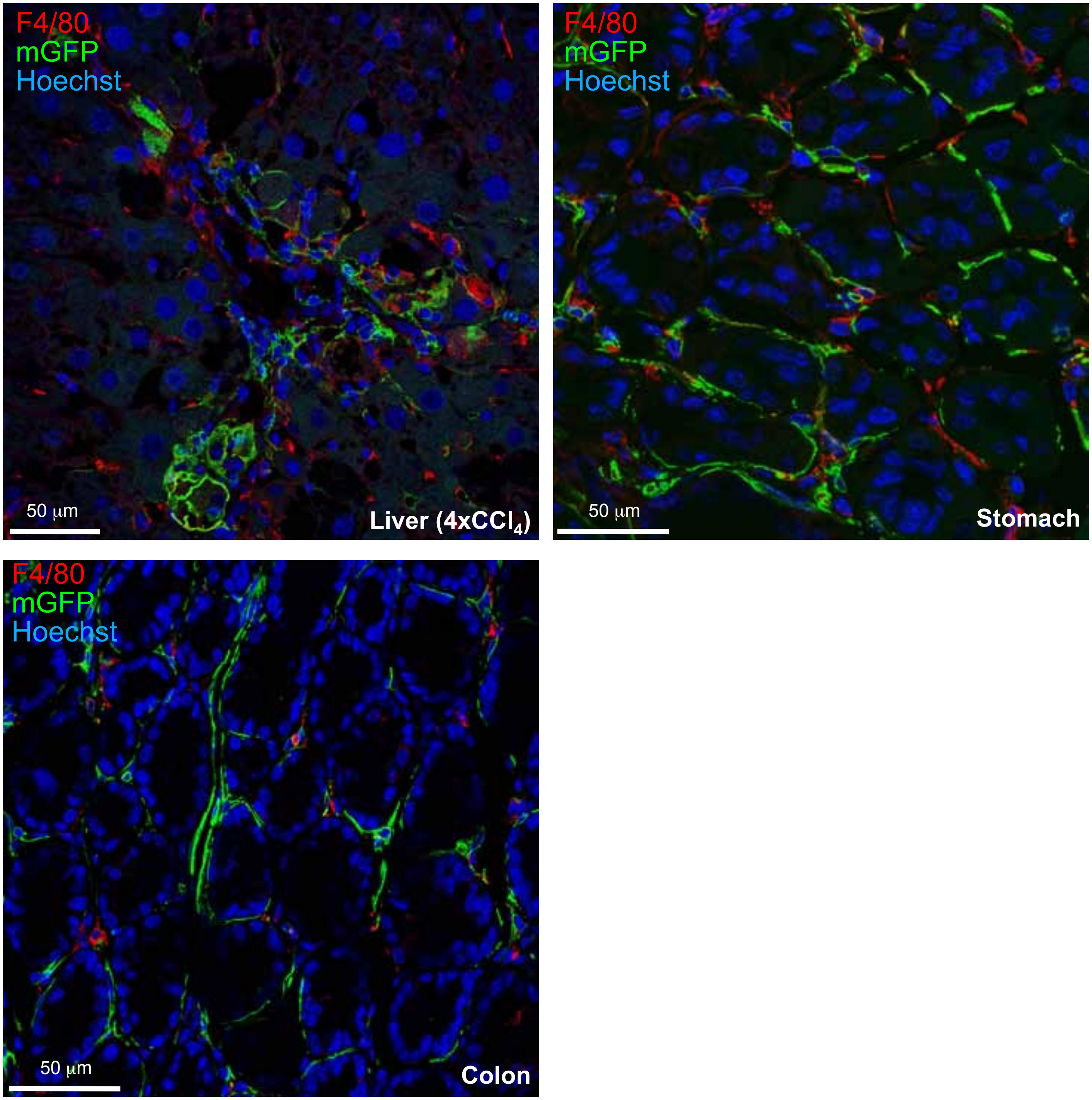
F4/80
mGFP
Hoechst
50 µm
Liver (4xCCl4)
F4/80
mGFP
Hoechst
50 µm
Stomach
F4/80
mGFP
Hoechst
50 µm
Colon

Suppl. Fig.5

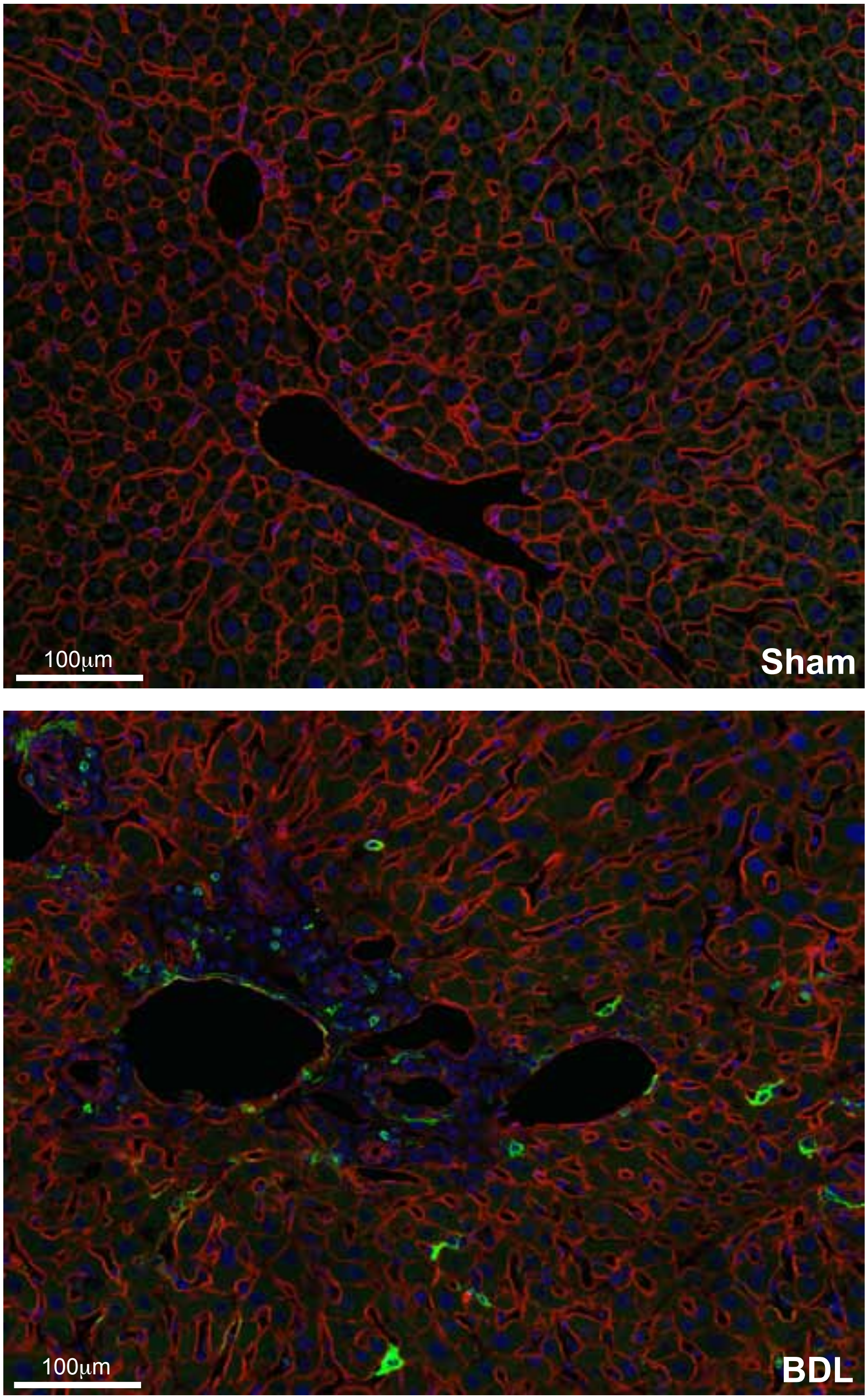

Suppl. Fig.6

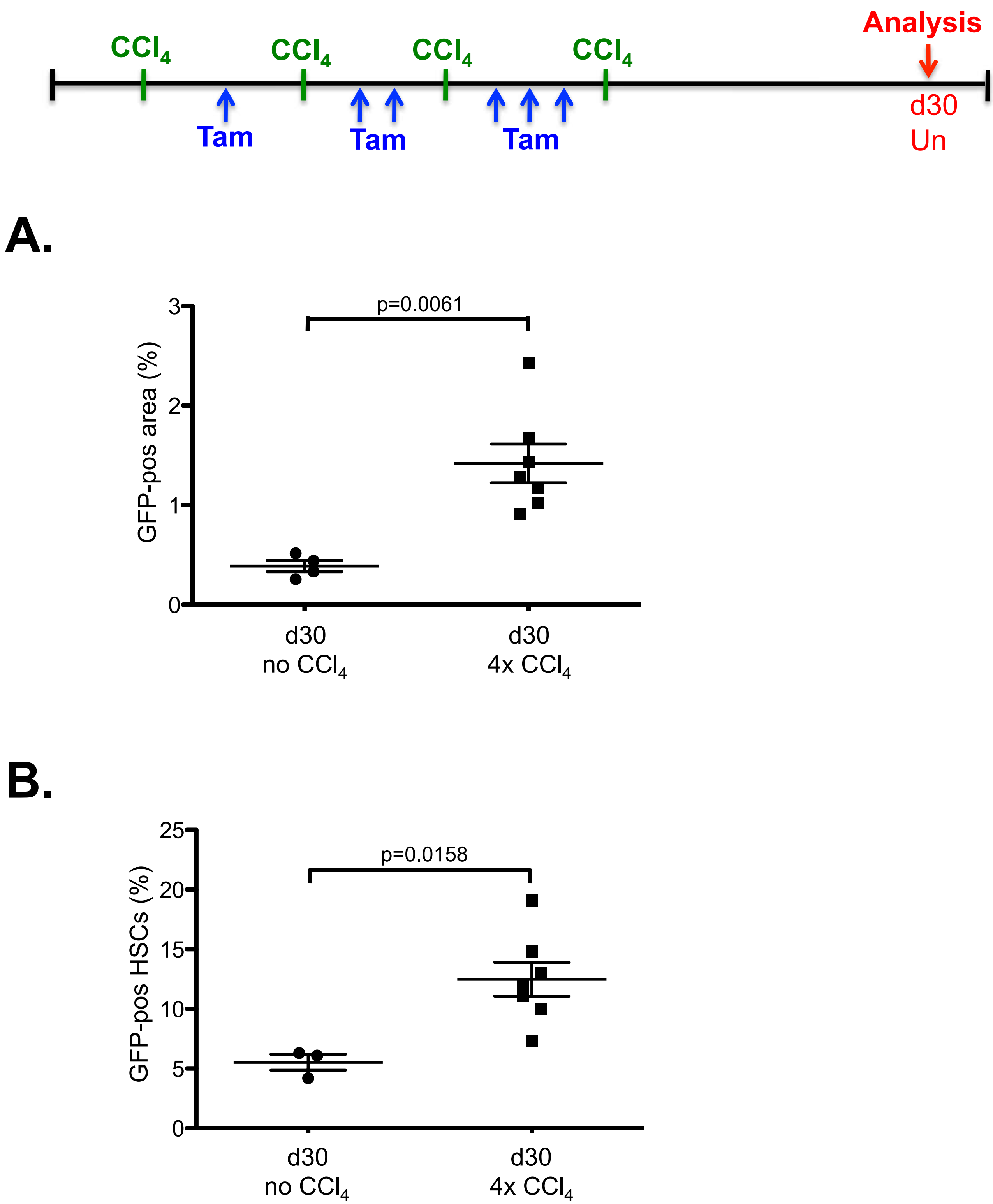
CCl4
CCl4
CCl4
CCl4
Analysis
Tam
Tam
Tam
d30
Un
A.
p=0.0061
GFP-pos area (%)
3
2
1
0
d30
no CCl4
d30
4x CCl4
B.
p=0.0158
GFP-pos HSCs (%)
25
20
15
10
5
0
d30
no CCl4
d30
4x CCl4

Suppl. Fig.7

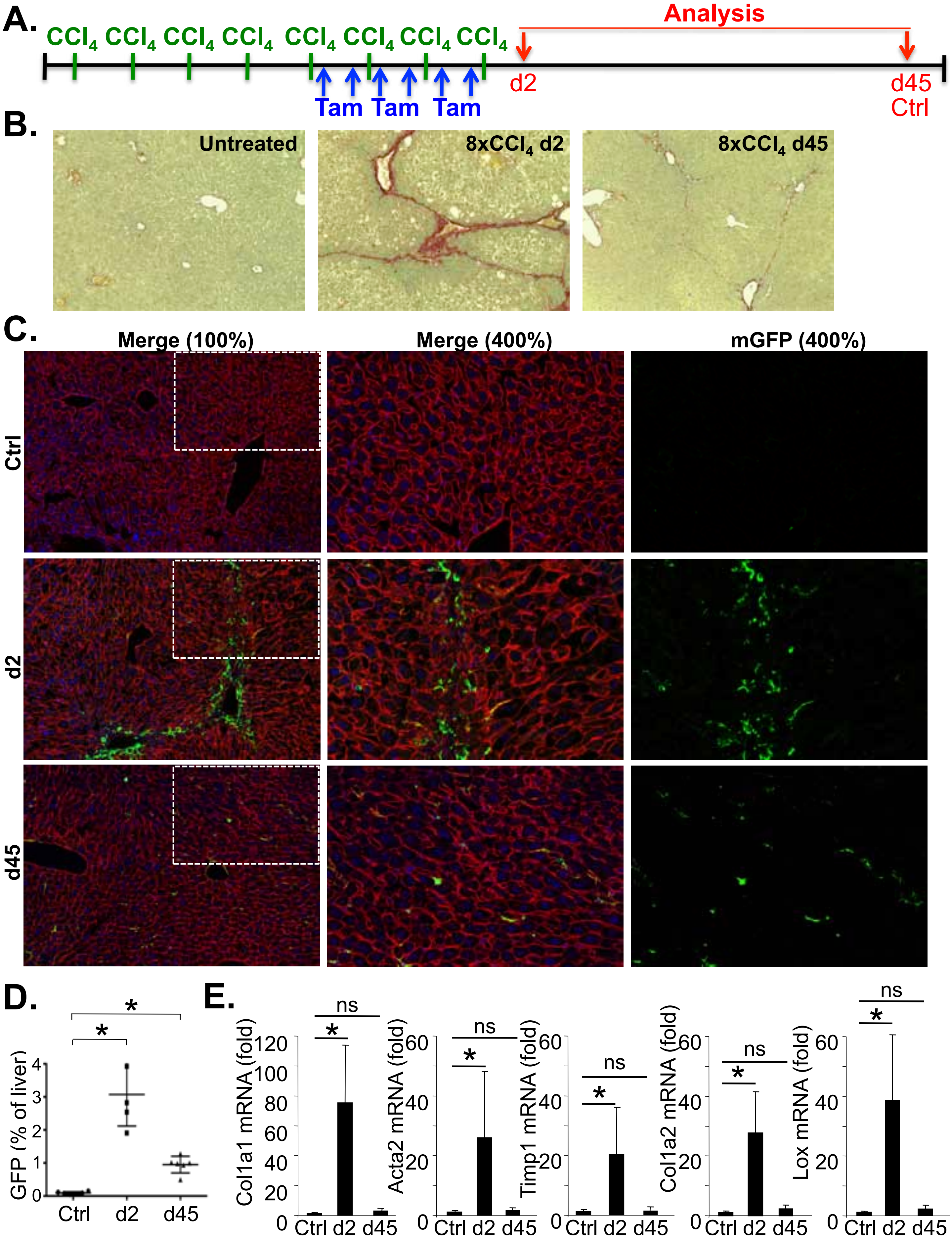

A.
CCl4 CCl4 CCl4 CCl4 CCl4 CCl4 CCl4 CCl4
Analysis
d2
d45
Ctrl
Tam Tam Tam
B.
Untreated
8xCCl4 d2
8xCCl4 d45
C.
Merge (100%)
Merge (400%)
mGFP (400%)
Ctrl
d2
d45
D.
GFP (% of liver)
Ctrl d2 d45
E.
Col1a1 mRNA (fold)
Acta2 mRNA (fold)
Timp1 mRNA (fold)
Col1a2 mRNA (fold)
Lox mRNA (fold)
ns
Ctrl d2 d45

Suppl. Fig.8

F.

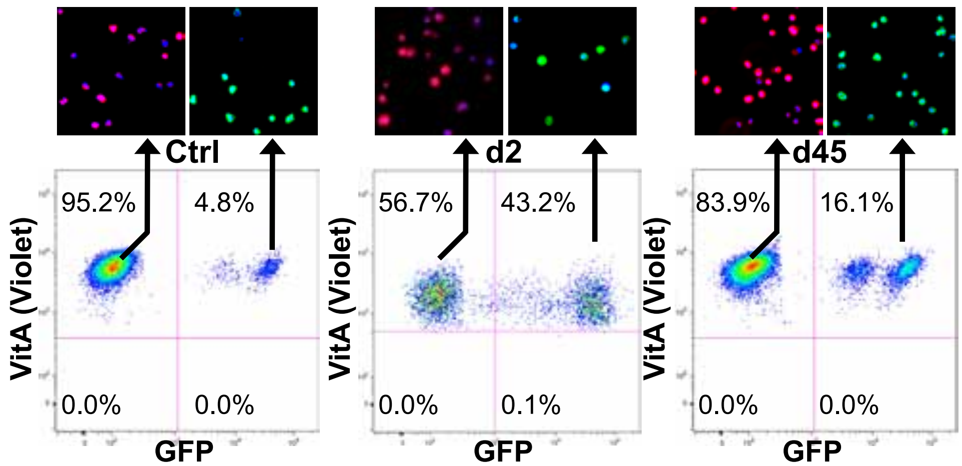

G.

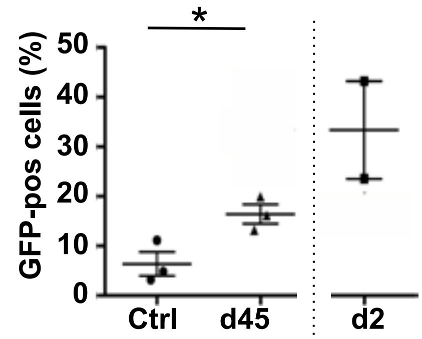

H.

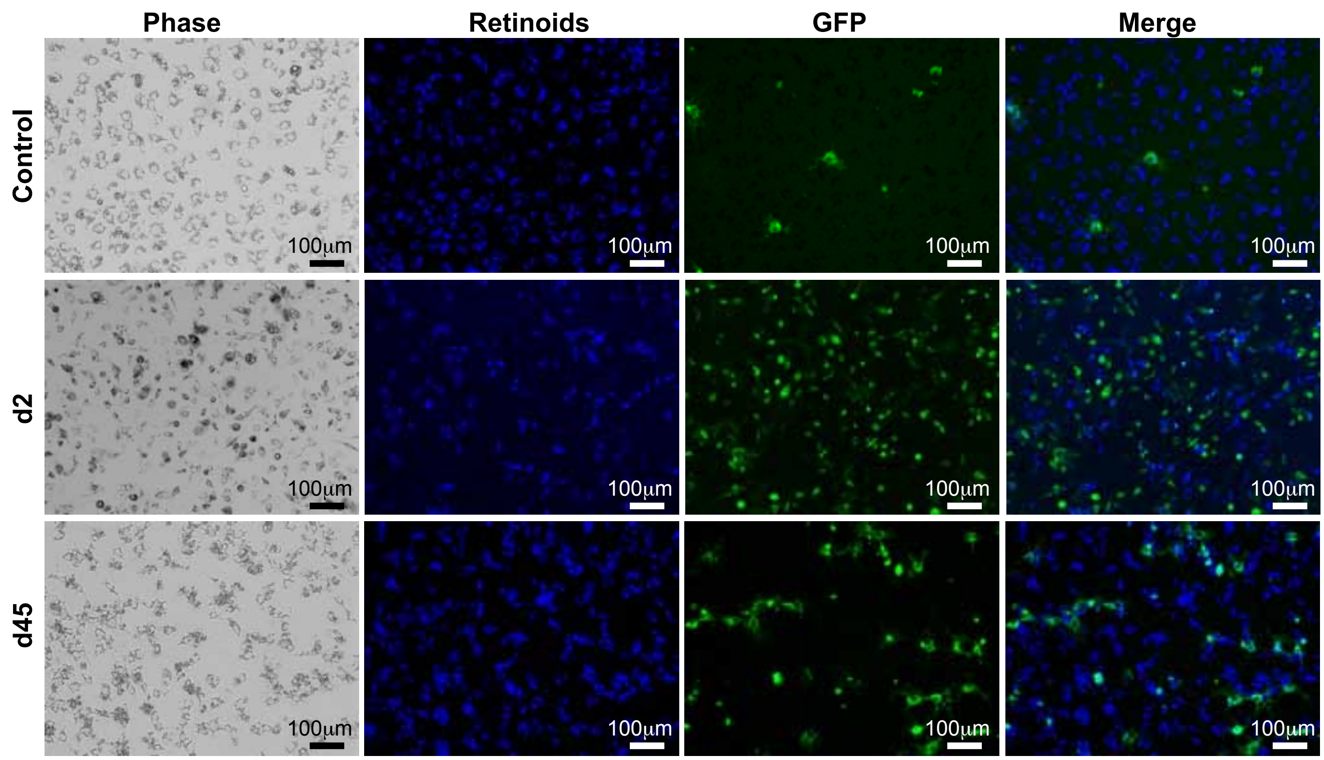

I.

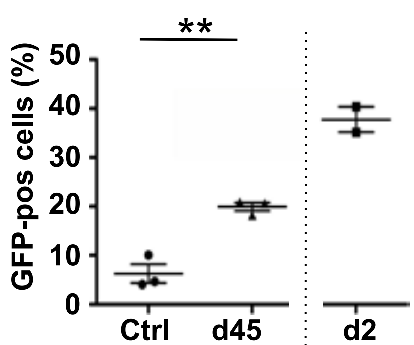

Suppl. Fig.8

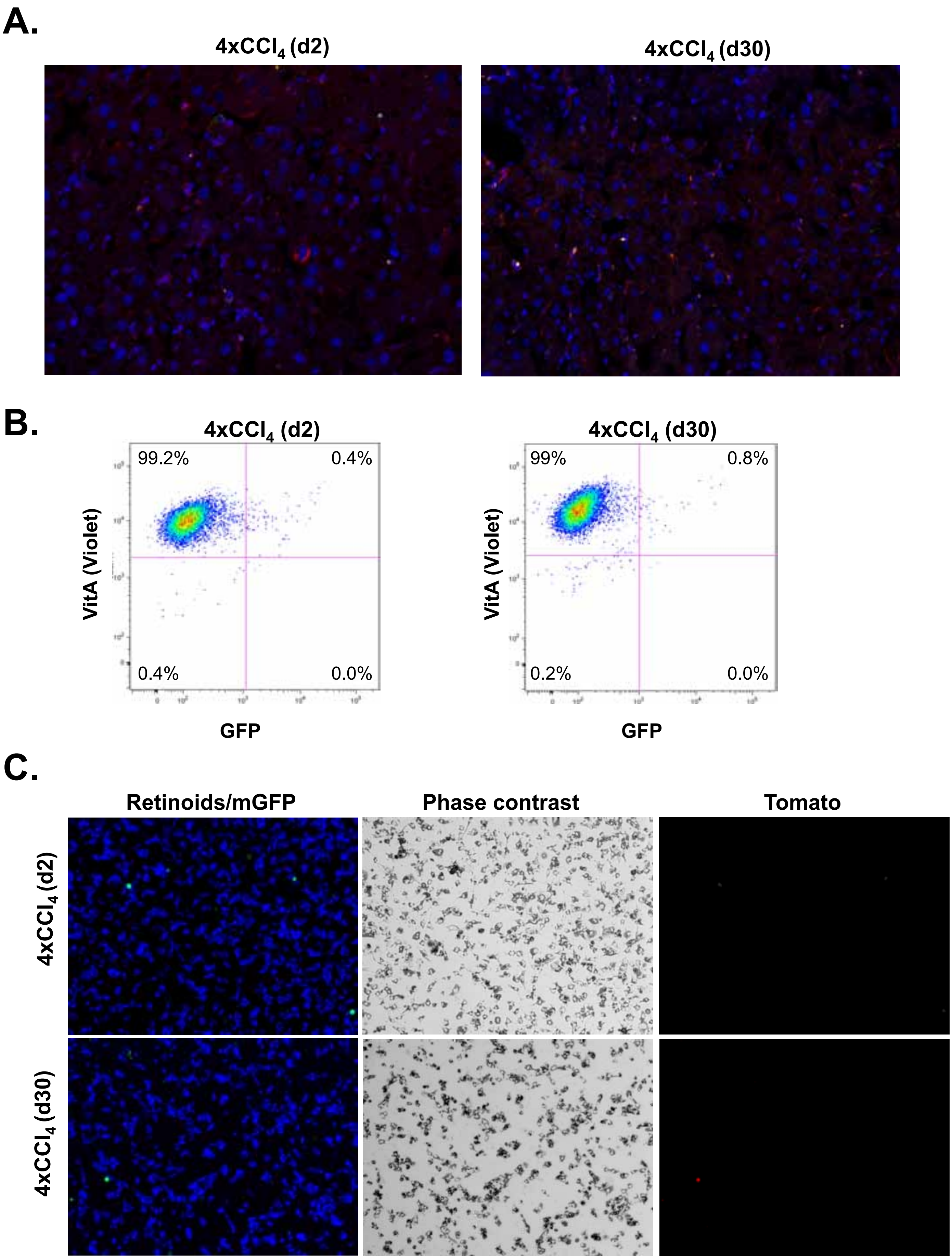
A.
4xCCl4 (d2)
4xCCl4 (d30)
B.
4xCCl4 (d2)
99.2%
0.4%
0.4%
0.0%
VitA (Violet)
GFP
4xCCl4 (d30)
99%
0.8%
0.2%
0.0%
VitA (Violet)
GFP
C.
Retinoids/mGFP
Phase contrast
Tomato
4xCCl4 (d2)
4xCCl4 (d30)

Suppl. Fig.9

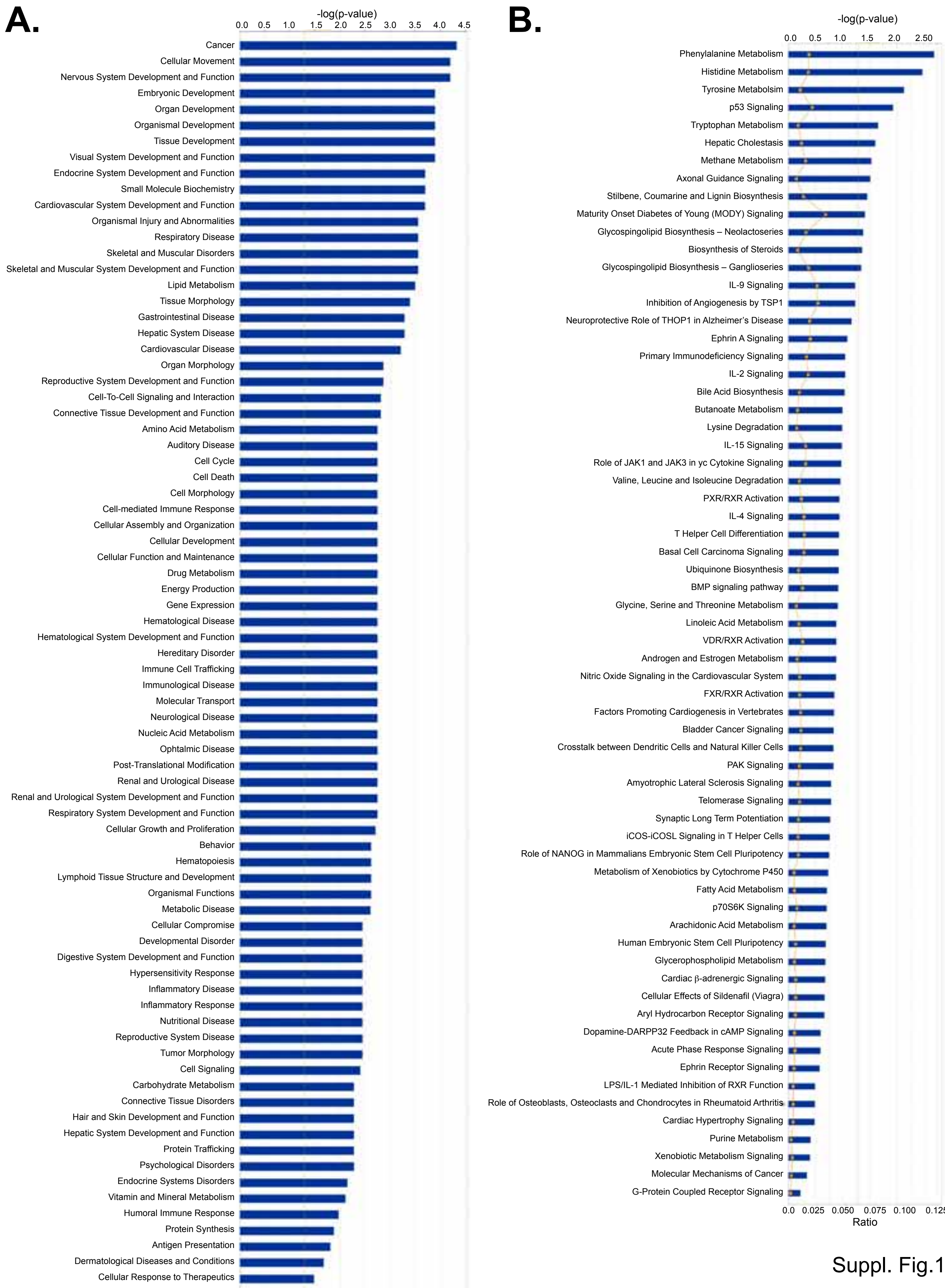
A.
-log(p-value)
0.0 0.5 1.0 1.5 2.0 2.5 3.0 3.5 4.0 4.5
Cancer
Cellular Movement
Nervous System Development and Function
Embryonic Development
Organ Development
Organismal Development
Tissue Development
Visual System Development and Function
Endocrine System Development and Function
Small Molecule Biochemistry
Cardiovascular System Development and Function
Organismal Injury and Abnormalities
Respiratory Disease
Skeletal and Muscular Disorders
Skeletal and Muscular System Development and Function
Lipid Metabolism
Tissue Morphology
Gastrointestinal Disease
Hepatic System Disease
Cardiovascular Disease
Organ Morphology
Reproductive System Development and Function
Cell-To-Cell Signaling and Interaction
Connective Tissue Development and Function
Amino Acid Metabolism
Auditory Disease
Cell Cycle
Cell Death
Cell Morphology
Cell-mediated Immune Response
Cellular Assembly and Organization
Cellular Development
Cellular Function and Maintenance
Drug Metabolism
Energy Production
Gene Expression
Hematological Disease
Hematological System Development and Function
Hereditary Disorder
Immune Cell Trafficking
Immunological Disease
Molecular Transport
Neurological Disease
Nucleic Acid Metabolism
Ophtalmic Disease
Post-Translational Modification
Renal and Urological Disease
Renal and Urological System Development and Function
Respiratory System Development and Function
Cellular Growth and Proliferation
Behavior
Hematopoiesis
Lymphoid Tissue Structure and Development
Organismal Functions
Metabolic Disease
Cellular Compromise
Developmental Disorder
Digestive System Development and Function
Hypersensitivity Response
Inflammatory Disease
Inflammatory Response
Nutritional Disease
Reproductive System Disease
Tumor Morphology
Cell Signaling
Carbohydrate Metabolism
Connective Tissue Disorders
Hair and Skin Development and Function
Hepatic System Development and Function
Protein Trafficking
Psychological Disorders
Endocrine Systems Disorders
Vitamin and Mineral Metabolism
Humoral Immune Response
Protein Synthesis
Antigen Presentation
Dermatological Diseases and Conditions
Cellular Response to Therapeutics
B.
-log(p-value)
0.0 0.5 1.0 1.5 2.0 2.50
Phenylalanine Metabolism
Histidine Metabolism
Tyrosine Metabolsim
p53 Signaling
Tryptophan Metabolism
Hepatic Cholestasis
Methane Metabolism
Axonal Guidance Signaling
Stilbene, Coumarine and Lignin Biosynthesis
Maturity Onset Diabetes of Young (MODY) Signaling
Glycospingolipid Biosynthesis – Neolactoseries
Biosynthesis of Steroids
Glycospingolipid Biosynthesis – Ganglioseries
IL-9 Signaling
Inhibition of Angiogenesis by TSP1
Neuroprotective Role of THOP1 in Alzheimer's Disease
Ephrin A Signaling
Primary Immunodeficiency Signaling
IL-2 Signaling
Bile Acid Biosynthesis
Butanoate Metabolism
Lysine Degradation
IL-15 Signaling
Role of JAK1 and JAK3 in yc Cytokine Signaling
Valine, Leucine and Isoleucine Degradation
PXR/RXR Activation
IL-4 Signaling
T Helper Cell Differentiation
Basal Cell Carcinoma Signaling
Ubiquinone Biosynthesis
BMP signaling pathway
Glycine, Serine and Threonine Metabolism
Linoleic Acid Metabolism
VDR/RXR Activation
Androgen and Estrogen Metabolism
Nitric Oxide Signaling in the Cardiovascular System
FXR/RXR Activation
Factors Promoting Cardiogenesis in Vertebrates
Bladder Cancer Signaling
Crosstalk between Dendritic Cells and Natural Killer Cells
PAK Signaling
Amyotrophic Lateral Sclerosis Signaling
Telomerase Signaling
Synaptic Long Term Potentiation
iCOS-iCOSL Signaling in T Helper Cells
Role of NANOG in Mammalians Embryonic Stem Cell Pluripotency
Metabolism of Xenobiotics by Cytochrome P450
Fatty Acid Metabolism
p70S6K Signaling
Arachidonic Acid Metabolism
Human Embryonic Stem Cell Pluripotency
Glycerophospholipid Metabolism
Cardiac β-adrenergic Signaling
Cellular Effects of Sildenafil (Viagra)
Aryl Hydrocarbon Receptor Signaling
Dopamine-DARPP32 Feedback in cAMP Signaling
Acute Phase Response Signaling
Ephrin Receptor Signaling
LPS/IL-1 Mediated Inhibition of RXR Function
Role of Osteoblasts, Osteoclasts and Chondrocytes in Rheumatoid Arthritis
Cardiac Hypertrophy Signaling
Purine Metabolism
Xenobiotic Metabolism Signaling
Molecular Mechanisms of Cancer
G-Protein Coupled Receptor Signaling
0.0 0.025 0.050 0.075 0.100 0.125
Ratio

Suppl. Fig.10

Supplementary Methods

Flow-cytometric analysis

For analysis of mGFP expression by microscopy, HSCs were plated in chamber slides and maintained for 16h in DMEM media containing 10% FBS and antibiotics. For flow-cytometric analysis of mGFP expression, HSCs were analyzed on a FACSAria cell sorter based on vitamin A fluorescence to gate high purity HSCs, and mGFP expression to detect HSCs marked by Vim-CreER, providing a percentage of mGFP-positive cells among all Vitamin A-positive cells. For the analysis of mRNA expression, HSCs were sorted on a FACSAria cell sorter based on vitamin A fluorescence to gate high purity HSCs, and in some cases mGFP expression, and immediately lysed in RNA lysis buffer.

Bone marrow transplantation. Bone marrow transplantation was performed as previously described [1]. Briefly, mice underwent lethal irradiation with 2x6Gy followed by intravenous injection of $10x10^6$ bone marrow cells and reconstitution for at least 2 months following transplantation.

Microarray analysis. Microarray analysis of quiescent HSCs (n=4 independent HSC isolates) and reverted HSCs (n=4 independent isolates) was performed using Affymetrix 1.0ST chips according to the manufacturers instructions. Briefly, 150 ng total RNA was used for cDNA sythesis and terminal labeling using the Ambion WT expression and terminal labeling kit and Robust Multichip Algorithm normalization [2]. Data was deposited in GEO (Accession number: GSE38648). Differential expression was obtained using Limma [3] in the R/Bioconductor statistical computing environment [4]. A significance cutoff of the Benjamini-Hochberg False Discovery Rate <0.05 was used [5]. Complete linkage hierarchical clustering [6] was performed on significant genes with $|\log_2 FC| > 0.67$ using Cluster 3.0 [7] and JavaTreeview [8]. Pathway analysis was done by IPA Ingenuity using genes selecting by the above criteria, i.e. False Discovery Rate <0.05 and $|\log_2 FC| > 0.67$.

Immunohistochemistry and confocal microscopy

Immunohistochemical staining was done on frozen sections using primary antibodies against vimentin (1:100, Epitomics, Burlingame, CA, USA), desmin (1:200, Lab Vision, Thermo Fisher Scientific, Fremont, CA, USA), F4/80 (1:200, AbD Serotec, Raleigh, NC, USA), rabbit-anti cow pankeratin ("wide spectrum screening", 1:200, DAKO, Carpinteria, CA, USA), CD31 (1:200, Pharmingen, San Diego, CA) and HNF4α (1:100, Santa Cruz Biotechnology, Santa Cruz, CA, USA), and secondary Alexa Fluor 647 goat anti-rabbit, chicken anti-rat or Alexa Fluor 660 donkey anti-goat (Invitrogen, Carlsbad, CA, USA). Confocal microscopy was performed on a Nikon A1R MP confocal microscope (Nikon Instruments, Melville, NY, USA) using a 40x oil immersion lens. For some pictures, 4-6 40x sections were merged.

mGFP quantification

mGFP expression in purified HSCs was quantified 16h after plating. mGFP and Vitamin A fluorescence and phase contrast images were visualized an Olympus 71IX microscope using a 10x lens. Vitamin A-positive cells, mGFP-positive cells and VitaminA-mGFP double-positive cells were counted in Adobe Photoshop. mGFP expression was detected in frozen liver sections by confocal microscopy and analyzed by Image J. Data is expressed as percentage of mGFP area in comparison to total area.

Quantitative Real-time and Single Cell PCR

After column purification of RNA (RNeasy, Qiagen), DNAse treatment and reverse transcription, mRNA levels of Acta2, Col1a1, Col1a2, Desmin, Lox and Timp1 were determined by quantitative real-time PCR on an Applied Biosystem 7300 PCR cycler using ABI Taqman primers and probes as described.[9,10] For single cell PCR, single HSCs were flow-cytometrically sorted, using Vitamin A autofluorescence and excluding dead cells by propidium iodide staining, into 96-well plates containing a 9 µl mix of RT buffer from the Invitrogen CellsDirectTM One−Step qRT−PCR kit (Invitrogen, Carlsbad, CA, USA) and primers for pre-amplification. For the construction of standard curves, 1000 HSCs were sorted into some wells. Reverse transcription and 18 cycles of pre-amplification were immediately performed after cell sorting using the CellsDirectTM One−Step qRT−PCR kit. The ensuing qPCR was performed as described above using the 7300 Applied Biosystems PCR cycler and Taqman probes. Single cell qPCR was normalized to desmin, and only desmin-positive wells were used for qPCR analysis.

Statistical analysis

All data is expressed as means with error bars representing the standard deviation. Statistical calculations were performed using Prism (Graphpad, San Diego California, USA). For comparison of two groups, two-sided unpaired t-test or Mann-Whitney test were used. For multiple group comparisons with normal distribution, ANOVA with Neuman-Keuls or Dunnett posthoc analysis was performed. A p-value < 0.05 was considered statistically significant.

Supplementary Figure legends.

Supplementary Figure 1. HSCs were isolated from male untreated Balb/c mice or from Balb/c mice treated with 4 injections of CCl_4 and sacrificed at various time points after the last CCl_4 injection for the analysis of fibrogenic genes Col1a1, Col1a2, αSMA and TIMP1.

Supplementary Figure 2. A. Balb/c mice were treated with 12 intraperitoneal injections of TAA or left untreated, followed by HSC isolation by the combination of gradient centrifugation and vitamin A-based single cell FACS sorting. Analysis included qHSCs from untreated mice (n=58) and HSCs 6 days after TAA (n=50), 12 days after TAA (n=102), and 24 days after TAA (n=58). Following preamplification, single cell qPCR was performed for Col1a1 (left panel). Shown is one out of two representative HSC isolations per time point. Sirius Red staining demonstrates TAA-induces fibrosis induction and reversal after cessation of injury. B. Vim-Cre mice were treated with 18 intraperitoneal injections of TAA and tamoxifen or tamoxifen alone as indicated, followed by HSC isolation by gradient centrifugation. Expression of mGFP was determined by flow-cytometric analysis of Vitamin A-autofluorescent HSCs. Shown are representative FACS images of each time point (left panels) and quantification (right panel) of HSCs isolated from control mice (n=6), HSCs isolated 3 days (n=4) and 45 days (n=3) after the last TAA injection. C-D. Expression of mGFP was determined by fluorescent microscopy of plated HSCs isolated from TAA-treated or tamoxifen only control mice at various time points. Shown are representative pictures of vitamin A fluorescence, mGFP expression and an overlay of both (C.), and a quantification (D.) of GFP-positive/Vitamin A-positive HSCs. E. Fibrogenic gene expression in whole liver from Vim-CreER mice was performed by qPCR in TAA-treated mice at day 3 (n=4) or day 45 (n=3) after the last CCl_4 injection or in mice receiving tamoxifen only ("Ctrl", n=6). * $p<0.05$, ** $p<0.01$

Supplementary Figure 3. Shown is the construct for generation of VimCreER-transgenic mice by BAC recombineering.

Supplementary Figure 4. To determine whether endothelial cells are marked in VimCreER transgenic mice, frozen sections of CCl_4-treated liver, stomach, small intestine and colon were stained for CD31 and analyzed by confocal microscopy. All sections show close but separate localization of CD31-positive endothelium (red) and mGFP (green). Nuclei were stained by Hoechst (blue).

Supplementary Figure 5. To determine whether macrophages are marked in VimCreER transgenic mice, frozen sections of CCl_4-treated liver, stomach and colon were stained for F4/80 and analyzed by confocal microscopy. All sections show close but separate localization of F4/80-positive macrophages (red) and mGFP (green). Nuclei were stained by Hoechst (blue).

Supplementary Figure 6. Confocal microscopy of livers from either 2 week bile duct ligated mice or sham-operated mice showing Vim-CreER mediated recombination by green mGFP fluorescence, and unrecombined cells by red mTom fluorescence. Nuclei were stainted by Hoechst (blue).

Supplementary Figure 7. A-B. Mice that either did or did not receive 4 injections of CCl_4 were sacrificed 31 days after their last tamoxifen injection (corresponding to 30 days after their last CCl_4 injection). Frozen liver sections were analyzed for the percentage of mGFP-positive area in mice that received CCl_4 (n=7) or mice that did not receive CCl_4 (n=4) (A.). HSCs were isolated from mice that received CCl_4 (n=7) or mice that did not receive CCl_4 (n=3) and the percentage of GFP-positive cells among all Vitamin A-positive cells was determined by counting (B.).

Supplementary Figure 8. A. Schematic diagram showing the timing of tamoxifen and CCl_4 injections, and sacrifice at 2, and 45 days after the last CCl_4 injection of VimCreER mice. B. Sirius Red images show almost complee reversal of liver fibrosis at d45 after 8 CCl_4 injections. C. mGFP and mTom expression in livers of untreated or CCl_4-treated mice were visualized by confocal microscopy 2, and 45 days after the last CCl_4 injection or a time point corresponding to 45 days after the last CCl_4 injection in the tamoxifen only control mice. The middle and right panel show higher magnification representing the area marked by dotted white lines in the left panel. D. mGFP expression was quantified and expressed as percentage of total area for CCl_4-treated mice at day 2 (n=6) or day 45 (n=5) after the last CCl_4 injection or mice receiving tamoxifen only ("Ctrl", n=6). E. Fibrogenic gene expression in whole liver from Vim-CreER mice was performed by qPCR in CCl_4-treated mice at day 2 (n=6) or day 45 (n=5) after the last CCl_4 injection or in mice receiving tamoxifen only ("Ctrl", n=6). F-G. HSCs were isolated from CCl_4-treated mice at d2 and d45 after last CCl_4 injection or from tams. HSCs from control mice receiving corn oil and tamoxifen only were isolated at a time corresponding to 45 days after the last CCl_4 injection. Expression of mGFP was determined by flow-cytometric analysis of Vitamin A-autofluorescent HSCs. Shown are representative FACS images of each time point (F.) and quantification (G.) of HSCs isolated from untreated mice (n=3), HSCs isolated 2 days (n=2) and 45 days (n=3) after the last CCl_4 injection. Inserts show HSCs from each sorted cell population confirming cells as vitamin A-positive HSCs that either do not express mGFP and are mTom positive, or express mGFP but not mTom. H-I. Expression of mGFP was determined by fluorescent microscopy of plated HSCs isolated from CCl_4-treated or tamoxifen only control mice at various time points. Shown are representative pictures of vitamin A fluorescence, mGFP expression and an overlay of both (H.), and a quantification (I.) of GFP-positive/Vitamin A-positive HSCs. * $p<0.05$ ** $p<0.01$

Supplementary Figure 9. Wild-type mice underwent bone marrow transplantation with mTom-mGFP+/Vim-CreER+ bone marrow as described in Methods and Material followed by 4 intraperitoneal injections of CCl_4 (0.5 µl/g body weight). A. Representative images at peak fibrosis (d2) and after fibrosis resolution (d30) show abundant bone mTom-positive marrow-derived inflammatory cells but only extremely rare mGFP-positive cell. B-C. HSCs were isolated from $4xCCl_4$-treated bone marrow-chimeric mice

2 and 30 days after the last CCl_4 injection. FACS analysis (B) and fluorescent microscopy (C) did not show significant presence of mGFP-positive HSCs.

Supplementary Figure 10. A-B. Display of the IPA pathway analysis for 37 genes that were altered in reverted HSCs in comparison to qHSCs fulfilling the criteria of False Discovery Rate <0.05 and $|log_2FC| > 0.67$. Show is the IPA analysis for gene functions (A) and canonical pathways (B) using the 37 genes with sign Supplementary Table 1.

Supplementary Table 1. Shown are the gene symbol, description, log fold change, p-value, corrected p-value ("fdr"), gene ontology biological process, gene ontology cellular component, gene ontology molecular function and pathway annotation for all 37 genes that were significantly different between reverted HSCs and qHSCs (fulfilling the criteria of False Discovery Rate <0.05 and $|log_2FC| > 0.67$).

Supplementary Table 2. Hepatic stellate cells were isolated from age-matched untreated mice (n=4) or mice that had undergone 4 CCl_4 injections followed by a 45 day recovery period (n=4) followed by microarray analysis using Affymetrix 1.0 ST arrays. Shown are all annoted genes with more than 0.5 log change and an uncorrected p-value of < 0.01.

Supplementary References

1. Dapito DH, Mencin A, Gwak GY, et al. Promotion of Hepatocellular Carcinoma by the Intestinal Microbiota and TLR4. Cancer Cell 2012;21:504-16.
2. Irizarry RA, Hobbs B, Collin F, et al. Exploration, normalization, and summaries of high density oligonucleotide array probe level data. Biostatistics 2003;4:249-64.
3. Smyth GK. Linear Models and Empirical Bayes Methods for Assessing Differential Expression in Microarray Experiments. Statistical Applications in Genetics and Molecular Biology 2004;3:Article 3, http://www.bepress.com/sagmb/vol3/iss1/art3/.
4. Gentleman RC, Carey VJ, Bates DM, et al. Bioconductor: open software development for computational biology and bioinformatics. Genome Biol 2004;5:R80.
5. Benjamini Y, Hochberg Y. Controlling the false discovery rate: a practical and powerful approach to multiple testing. Journal of the Royal Statistical Society 1995;57:289-300.
6. Everitt BS, Landau S, Leese M. Cluster Analysis. Arnold, 2001.
7. de Hoon MJ, Imoto S, Nolan J, et al. Open source clustering software. Bioinformatics 2004;20:1453-4.
8. Saldanha AJ. Java Treeview--extensible visualization of microarray data. Bioinformatics 2004;20:3246-8.
9. Kluwe J, Pradere JP, Gwak GY, et al. Modulation of hepatic fibrosis by c-Jun-N-terminal kinase inhibition. Gastroenterology 2010;138:347-59.
10. Seki E, De Minicis S, Osterreicher CH, et al. TLR4 enhances TGF-beta signaling and hepatic fibrosis. Nat Med 2007;13:1324-32.